ISPARTA UYGULAMALI BİLİMLER ÜNİVERSİTESİ

Uluslararası Teknolojik Bilimler Dergisi
International Journal of Technological Sciences
Elektronik Dergi, e-ISSN: 1309-1220
VOLUME / CİLT 16 ISSUE / SAYI 2 DECEMBER / ARALIK 2024
UTBD IJTS

Uluslararası Teknolojik Bilimler Dergisi

International Journal of Technological Sciences

Yayımcı / Publisher

Isparta Uygulamalı Bilimler Üniversitesi

Grafik Tasarım / Graphic Design
Sinan İLKAZ

Teknik Sorumlu / Technical Manager
Nejat TÜKENMEZ

Mizanpaj / Make-up
Dr. Serpil ÇELİK TOKER

Dergi Adresi / Journal Address
Uluslararası Teknolojik Bilimler Dergisi Editörlüğü
Isparta Uygulamalı Bilimler Üniversitesi
Teknoloji Fakültesi
32260, Batı Kampüsü, Isparta, Türkiye
Tel: +90 246 2111569
Fax : +90 246 2111984
E-posta/E-mail: utbd@isparta.edu.tr

Uluslararası Teknolojik Bilimler Dergisi, Isparta Uygulamalı Bilimler Üniversitesi tarafından yılda 3 sayı elektronik olarak yayınlanmaktadır.
International Journal of Technological Sciences is published three times a year electronically by Isparta University of Applied Sciences.

Cilt/Volume: 16	Sayı/Issue: 2	Aralık/December 2024

e - ISSN : 1309-1220

ISPARTA UYGULAMALI BİLİMLER ÜNİVERSİTESİ

Uluslararası Teknolojik Bilimler Dergisi
International Journal of Technological Sciences
Elektronik Dergi, e-ISSN: 1309-1220
VOLUME / CİLT 16 ISSUE / SAYI 2 DECEMBER / ARALIK 2024
UTBD IJTS

İÇİNDEKİLER / CONTENTS Sayfa No / Page No

Araştırma Makalesi / Research Article

*Uluslararası Teknolojik Bilimler Dergisi, **Google Scholar** ve **EBSCO** tarafından taranmaktadır. https://www.ebsco.com/title-lists adresinde "Academic Search Premier" listesinde yer almaktadır.*
*International Journal of Technological Sciences is indexed by **Google Scholar** and **EBSCO**. It is included in "Academic Search Premier" at the address https://www.ebsco.com/title-lists*

ISPARTA UYGULAMALI BİLİMLER ÜNİVERSİTESİ

Uluslararası Teknolojik Bilimler Dergisi

International Journal of Technological Sciences

UTBD IJTS

Research Article/Araştırma Makalesi

Usage of different modulation applications in OFDM systems and performance comparison

Özkan Sezer[1], **Nihat Daldal**[*2], **İbrahim Yücedağ**[1]

[1]Düzce Üniversitesi, Lisansüstü Eğitim Enstitüsü, Elektrik Elektronik Bilgisayar Mühendisliği, Düzce, Türkiye
[2]Bolu Abant İzzet Baysal Üniversitesi, Elektrik Elektronik Mühendisliği, Bolu, Türkiye

Keywords
OFDM
Ber
Digital modulation

Article history:
Received: 27.08.2024
Accepted: 03.12.2024

Abstract: OFDM (orthogonal frequency division multiplexing) systems are the most efficient use of today's radio frequency spectrum. The system is the simultaneous splitting of a signal into small signals and sending them to the receiver. It is mainly a need in high-capacity data transfer and multi-user systems. Depending on the usage purpose, the OFDM method provides a data transmission with maximum accuracy at the highest speed as long as an appropriate and high-performance modulation type is used. This study performed an FDM communication simulation primarily for multiple data transmissions over a single line. After selecting the carrier frequencies used in FDM, the necessity of the OFDM communication method is proved when considering the high quality of the communication. In the next phase, performance comparisons were made by calculating the BER (Bit error rate) value at different SNR (signal to noise ratio) and multipath fading values of the modulations used in the OFDM method. Specific variable values that the modulation type providing the highest accuracy data transmission has been determined in this study. As a result of the comparison, the best BER value at 8-way communication and 0 SNR was found at 0.28 in the BPSK modulation type. In 8-way transmission and 30 SNR measurements, the lowest BER value was 0.016. In all comparisons made among the used modulation types 'BPSK, QPSK, 8PSK, 16QAM, 32QAM, 64QAM', the lowest BER values were determined in the BPSK modulation type.

To Cite/Atıf için: Sezer Ö. Daldal N. Yücedağ İ. Usage of different modulation applications in OFDM systems and performance comparison. International Journal of Technological Sciences, 16(2), 33-43, 2024.

OFDM sistemlerinde farklı modülasyon uygulamalarının kullanımı ve performans karşılaştırması

Anahtar Kelimeler
OFDM
Ber
Sayısal Modülasyon

Makale geçmişi:
Geliş Tarihi: 27.08.2024
Kabul Tarihi: 03.12.2024

Öz: OFDM (ortogonal frekans bölmeli çoğullama) sistemleri günümüz radyo frekans spektrumunun en verimli kullanımıdır. Sistem, bir sinyalin eş zamanlı olarak küçük sinyallere bölünerek alıcıya gönderilmesidir. Özellikle yüksek kapasiteli veri iletimi ve çok kullanıcılı sistemlerde ihtiyaç duyulmaktadır. OFDM yöntemi, kullanım amacına bağlı olarak, uygun ve yüksek performanslı bir modülasyon tipi kullanıldığı takdirde en yüksek hızda maksimum doğrulukla veri iletimi sağlamaktadır. Bu çalışmada, öncelikle tek bir hat üzerinden çoklu veri iletimi için bir FDM haberleşme simülasyonu gerçekleştirilmiştir. FDM'de kullanılan taşıyıcı frekansları seçildikten sonra, haberleşmenin yüksek kalitesi de göz önüne alındığında OFDM haberleşme yönteminin gerekliliği kanıtlanmıştır. Bir sonraki aşamada, OFDM yönteminde kullanılan modülasyonların farklı SNR (sinyal gürültü oranı) ve çok yollu sönümlenme değerlerinde BER (Bit hata oranı) değeri hesaplanarak performans karşılaştırmaları yapılmıştır. Bu çalışmada, en yüksek doğrulukta veri iletimini sağlayan modülasyon tipinin belirli değişken değerleri belirlenmiştir. Karşılaştırma sonucunda 8 yollu haberleşme ve 0 SNR'da en iyi BER değeri 0,28 olarak BPSK modülasyon tipinde bulunmuştur. 8 yollu iletim ve 30 SNR ölçümünde ise en düşük BER değeri 0,016 olmuştur. Kullanılan modülasyon tipleri 'BPSK, QPSK, 8PSK, 16QAM, 32QAM, 64QAM' arasında yapılan tüm karşılaştırmalarda en düşük BER değerleri BPSK modülasyon tipinde belirlenmiştir.

* İlgili yazar/Corresponding author: nihatdaldal@ibu.edu.tr

1. Introduction

OFDM is a multi-carrier communication system that provides narrowband transmission with multiple carrier signals [1]. OFDM is similar to FDM (Frequency division multiplexing), allowing multiple user logins by dividing the available bandwidth into many channels [2]. However, in the OFDM method, as seen in Fig.-1, higher efficiency is reached when a carrier is closer to the other. In this case, a phase difference of 90 degrees is created to avoid interference between carriers. In this communication method, the 90-degrees phase difference between carriers is realized by Inverted Fast Fourier Transform (IFFT) in transmitters [3]. Each carrier is modulated separately, and all modulated signals are transmitted in the same bandwidth. The most used modulation techniques in OFDM communication are PSK (phase-shifted switching), which provides the phase of the carrier signal, QAM (quadratic amplitude modulation), which provides data transmission according to the amplitude and phase change of the signal [4][5]. All carriers are collected at the transmitter output and sent to the transmission channel when any modulation techniques are used. Just as the incoming signal is taken, the signal is transformed to the frequency spectrum by the Fast Fourier Transform (FFT) on the receiving side. The information signals are decomposed and converted to their original form using a balanced modulator for each carrier. As it is well-known, OFDM communication is used in digital communication systems such as WLAN, LTE, DVB-T, and 5G [6][7][8]. Thanks to the more efficient use of bandwidth, more users are accessed in each channel. In passband modulations (ASK, FSK, PSK), data transmission is carried out by successive transmission of each symbol [9][10]. The symbol for belonging to each bit used in modulation uses the entire frequency spectrum. As the communication speed increases, the symbol rate should be reduced. In this case, the spectral components of each symbol interfere with each other on the receiving system side; this is called ISI (inter-symbol interference) effect [11]. The spread of signals in the time spectrum also creates an ISI effect, and negative effects increase the BER rate on the receiver side. The energy of each symbol affects the energy of the neighboring symbol. This is seen in PDF (power density factor) graphics of symbols [12]. In this case, the channel selectivity decreases in the receiver systems. In passband modulations, instead of sending data of certain bit lengths step by step in a large time slot with a single carrier, sending a carrier to each group with the formed bit groups also increases the communication speed. By multiplying the number of bits grouped here, the communication speed increases by the number of carriers. The larger the number of carriers, the longer the time used for each symbol. Thus, the ISI effect is also reduced. The basic principle of the OFDM communication technique is based on this sub-channel method. Data is transmitted with selected subcarriers at frequencies very close to each other. The 90-degree phase difference between the carriers allows the carriers to be selected at very close frequencies. Compared to classical methods, the frequency band used by subcarriers is narrower. This way, the number of grouped bits is increased by using more subcarriers. In the literature studies, by comparing the performance of four different modulation types in Sharma et al.'s OFDM system, the BER ratios ranged from 0.4 to 0.9. [13]. Thai et al. studied estimating the BER analysis of QPSK modulation on the OFDM system [14]. Hoxha et al. examined the performance of only QPSK and 16QAM modulations in the OFDM communication system at different SNR ratios in their study [15]. In this study, six different modulation types (BPSK, QPSK, 8PSK, 16QAM, 32QAM, 64QAM), six different SNRs (0,5,10,15,20,30) and four multipath (1,2, 4,8) performances were compared using the OFDM system. The biggest advantage of this research over existing studies is communication was carried out by changing the SNR and multipath (multipath communication channel) via the OFDM system by using the most frequently used modulation techniques (BPSK, QPSK, 8PSK, 16QAM, 32QAM, 64QAM) and CP (Cyclic Prefix) constant [16]. As a result of the study, the BER performances of each modulation technique were compared separately. Different simulation applications have been made in variable SNR, Multipath, and modulation types, and it has been revealed which modulation type is more efficient in which situations.

2. Basic block diagram of OFDM method

OFDM basic block diagram is shown in Fig. 1.

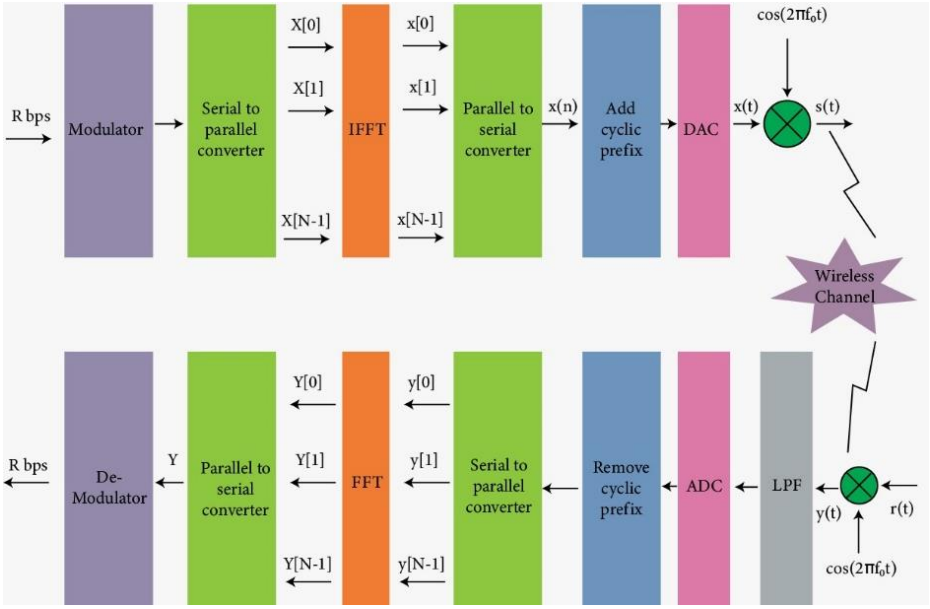

Figure 1. Basic block diagram of OFDM system [17]

The data used in the system is a random numeric bit generator. The aim here is to reproduce the produced bit series in the last layer of the receiver part. The modulation used in the OFDM communication system is modulated by the bit series produced in the desired size, depending on the type. Modulation types such as PAM, QPSK, QAM, 16PSK, BPSK can be used as needed. The modulated signal is split into as many parallel segments as it needs to be divided into carriers. These subcarriers form the frequency multiplexing part. The number of carriers can be 2n (4, 8, 16, 32, 64). The signal converted into parallel blocks is converted into signals perpendicular to each other by taking the inverse Fourier to transform separately. The operation in Fig. 2 constitutes the main part of the OFDM system. Perpendicular symbols allow maximum carrier transmission within the transmission band.

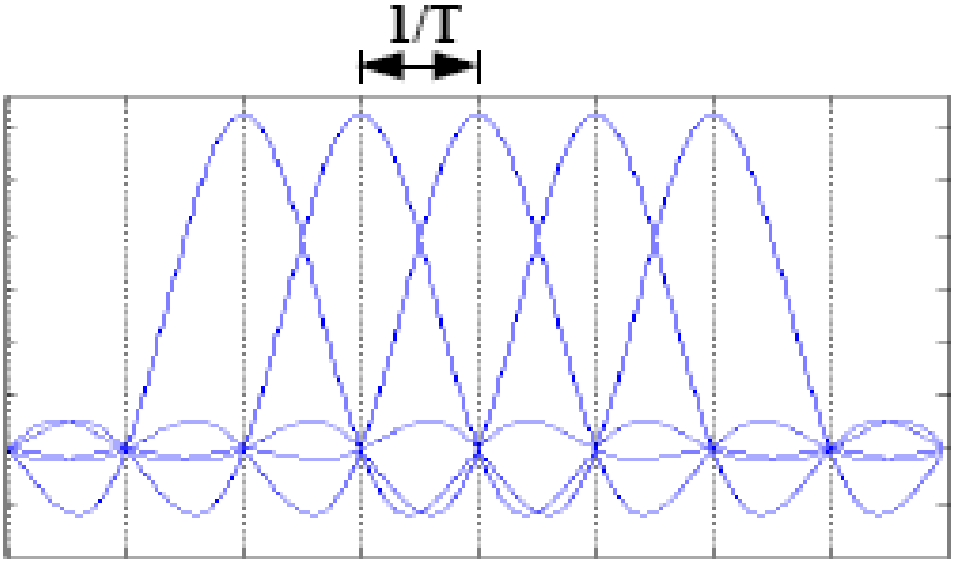

Figure 2. OFDM transmission spectrum

Adding the end of the signal to the beginning of the signal to prevent time shifts between symbols is called Cyclic Prefix insertion. This situation is used to avoid carrier interaction (ICI) and inter-symbol interaction (ISI) that occur in signal transmission [16][18].

In OFDM communication, time-frequency domain transformations are performed in Fourier transform operations on the transmitter and receiver sides. When expressed in the equation;
OFDM encoding processing applies the IFFT. This method:

Encode (IFTT Processing):

frequency domain samples → time-domain sample

$$x(t) = \sum_{k=N/2}^{\frac{N}{2}-1} X[k]e^{j2\pi kt/N} \quad (1)$$

Time-domain Frequency- domain

$$X[k] = \frac{1}{N}\sum_{t=N/2}^{\frac{N}{2}-1} x(t)e^{-j2\pi kt/N} \quad (2)$$

Decode (FFT Processing): time-domain samples frequency domain sample;

Orthogonality of any two bits:

$$\sum^{\frac{N}{2}-1} e^{-j2\pi kt/N} e^{-j2\pi pt/N} = 0, \forall p \neq k \quad (3)$$

The IFFT transformation ensures that the carriers are orthogonal on the transmitter side.

3. Different modulation techniques

3.1. PSK Modulation

In phase-shift keying (PSK), the binary signal to be transmitted changes the phase of the sine signal depending on whether 0 or 1. PSK modulation is one of the modulation types that is least affected by noise. For this reason, it is used in satellite communication and high-speed digital communication systems. There are varieties such as BPSK, QPSK, 8PSK. For example, BPSK can be expressed by the following mathematical equation.

If numeric 0 is to be sent:

$$A\cos(\omega t + \pi) = -A\cos(\omega t) \quad (4)$$

If numeric 1 is to be sent:

$$A\cos(\omega t) \quad (5)$$

In the phasor space, it appears as in Fig. 3.

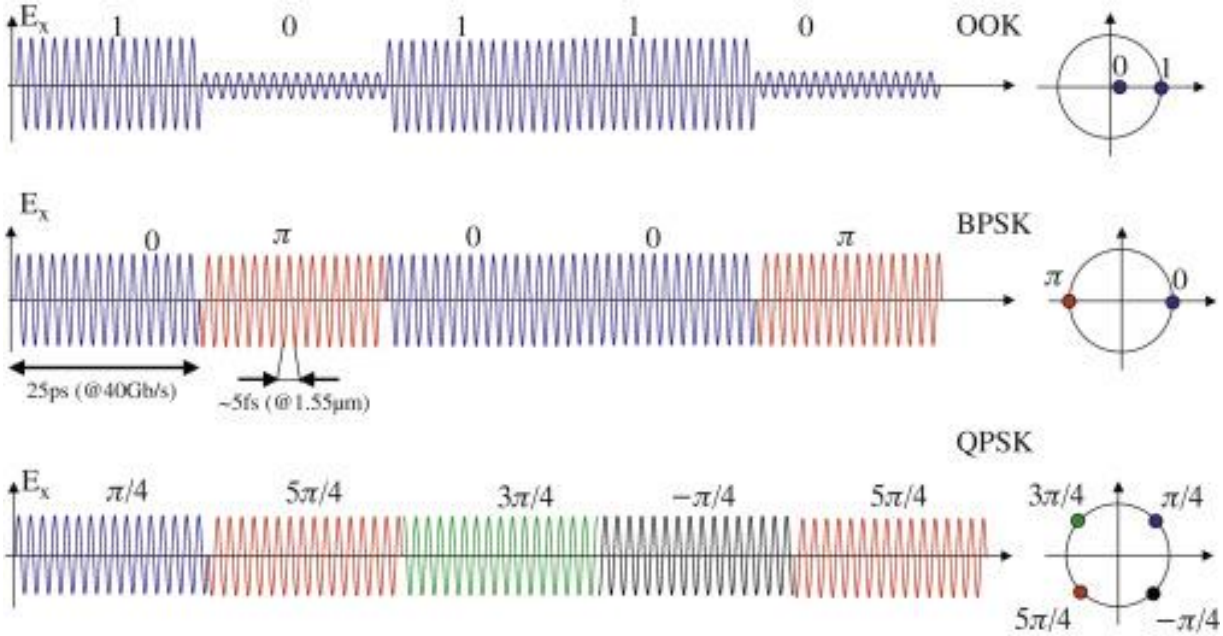

Figure 3. PSK Phasor space shapes

3.2. QAM Modulation

Quadrature amplitude modulation QAM (quadrature amplitude modulation) is a combination of amplitude modulation and PSK modulation. It is a type of modulation that contains phase and amplitude information to express a signal. It is expressed with numbers such as 16 QAM, 32 QAM, 64 QAM. 16 QAM = 4 amplitude levels + 4 different phases. Generally, the purpose of use; is to transmit different signals in different phases with a single carrier. Today, due to the development of signal processing and communication electronics techniques and the need for more information transmission, it is mostly used as 256 QAM [2]. QAM modulation in each sub-channels formed by the DMT modulation used in the ADSL connection type can be given as an example of the above type of use. It is obtained by placing the carriers to form a square in the phasor space.

4. Implementation of basic FDM modulation simulation and OFDM requirement

FDM effectively allows for the simultaneous transmission of multiple signals by utilizing distinct frequency bands, ensuring that each signal can be retrieved without interference during the demultiplexing process. When FDM expressed in the equation 4 and basic part of the balanced modulator(multiplier) shown in Fig-4. In Fig. 5, the simulation application of the FDM communication system, which forms the basis of the OFDM communication system, is seen. In addition, 4 separate low-frequency information signals were collected by modulating in a balanced modulator with four respective carriers signals and applied to the transmission line. On the receiving side, each channel was filtered with a coherent type receiver, and four separate information signals were obtained again.

$$S(t) = \sum_{i=1}^{n} s_i(t).\cos(2\pi f_i t) \quad (4)$$

Where:
(t) is the combined signal.
(t) are the individual signals.
are the corresponding carrier frequencies for each signal.

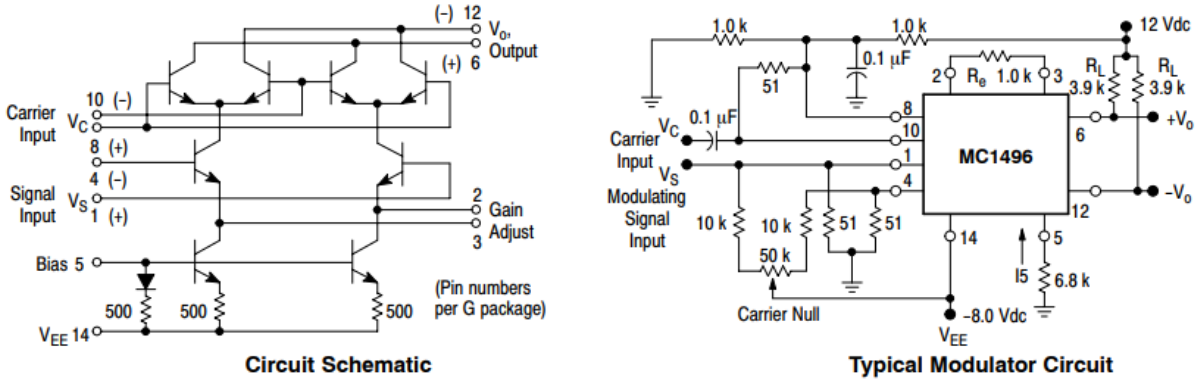

Figure 4. Balanced modulator circuit

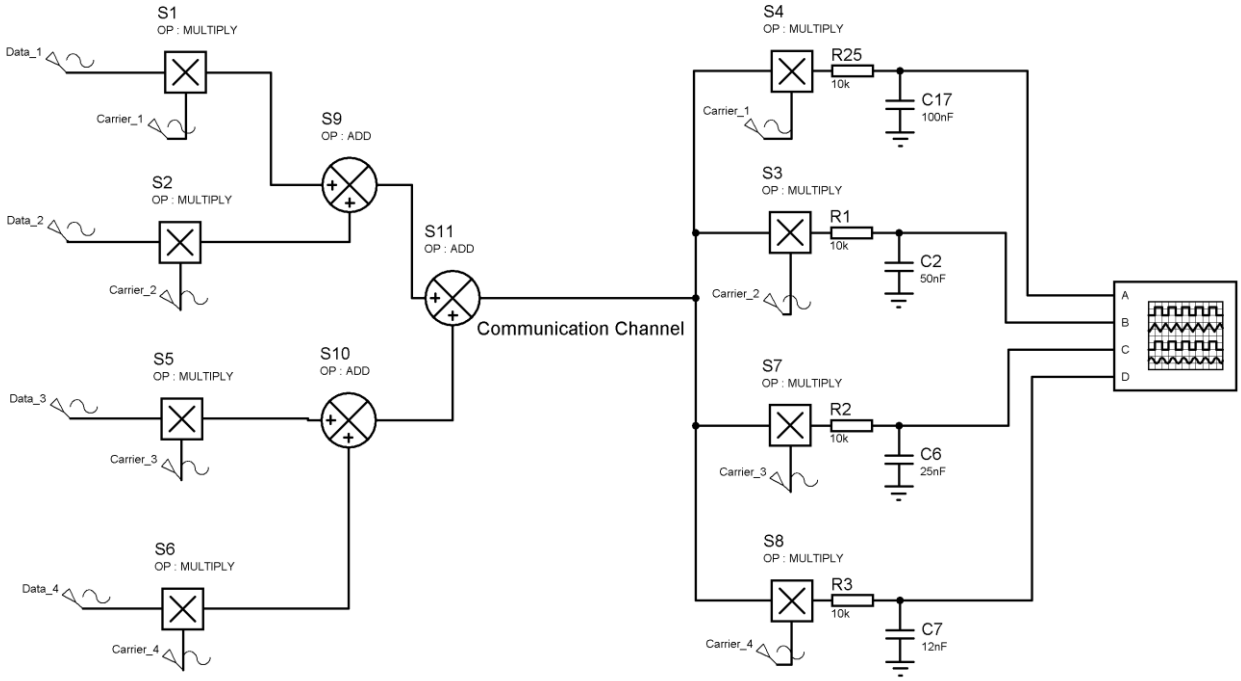

Figure 5. FDM Communication simulation

As shown in Fig. 6, when the system bandwidth is too narrow, that is, when the carrier frequencies are too close to each other, channel information is mixed on the receiving side. For this reason, OFDM has been the reason for choosing to communicate from a single channel using minimum bandwidth [25]. In Table 1, the carrier frequencies selected close to each other are shown to prove data interference in FDM communication.

In order to show the correct transmission of information signals in communication and to see

them separately visually, their frequencies were selected differently.

Table 1. Frequencies selected for minimum BW in FDM communication

Carrier Frequency	Information signal Frequency
10 kHz	10 Hz
10.2 kHz	20 Hz
10.3 kHz	30 Hz
10.4 kHz	40 Hz

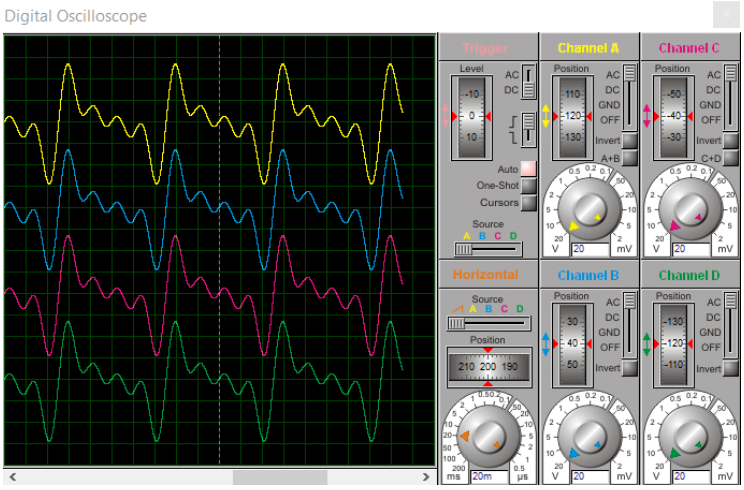

Figure 6. Signals obtained in 4 separate channels on the receiving side when carrier frequencies are selected too close for minimum BW

Fig. 7 shows that four separate information signals received from a single channel in FDM communication are separated adequately at the receiving point when the carrier frequencies are selected far from each other.

In Table 2, it is seen that the carrier frequencies are selected far from each other.

Table 2. Different carrier frequencies to avoid data interference

Carrier Frequency	Information signal Frequency
10 kHz	10 Hz
12 kHz	20 Hz
14 kHz	30 Hz
16 kHz	40 Hz

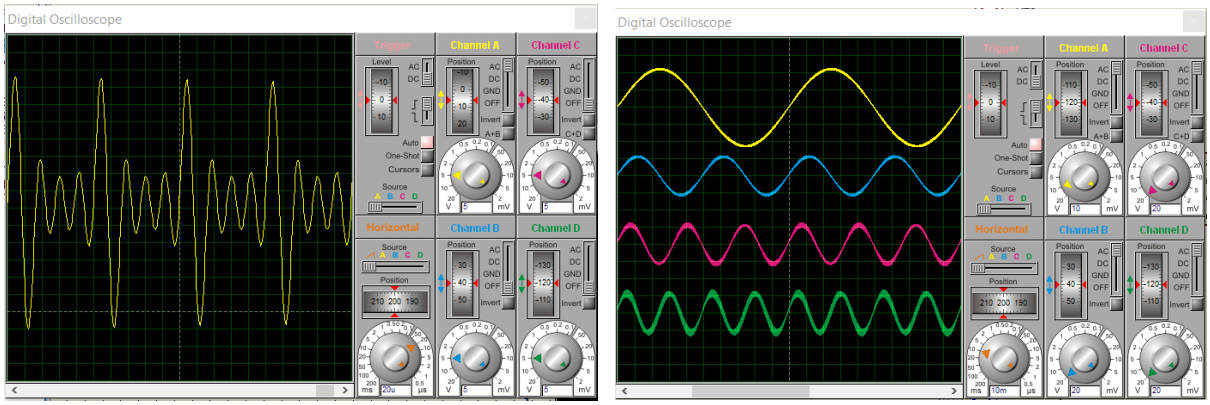

Figure 7: FDM communication signal and four separate information signals obtained on the receiving side

Because selecting carrier frequencies far from each other in FDM communication increases bandwidth, its frequencies can be chosen close to each other by making the carriers perpendicular to each other (OFDM). Thus, the bandwidth used is minimal.

5. Efficiency (performance) analysis of modulation techniques

The two most efficient modulations in the OFDM technique were examined. In these modulation types, Multipath (multipath) and SNR (signal to noise ratio) are taken as variables; BER (bit error rate) was calculated by comparing the signal at the receiver output with the original signal as a result of six different modulations, respectively simulation. Other variables Cyclic Prefix (CP) 16, FFT size 64, channel estimation method LS (Least Square), are taken as constant in the simulation program. The values obtained from seventy-two (72) different simulations have been interpreted [19].

5.1. BPSK Modulation

In the simplest form of PSK, the digital input signal alternates between 1 and 0, while the carrier's output phase shifts between two angles 180° apart. In the simulation, taking Multi-Path from 1 to 8 (1, 2, 4, 8 values), SNR (Signal-to-Noise Ratio) 0 to 30 dB (0 dB, 15 dB, 30 dB values), respectively. results have been recorded [20]. Here, the results of the highest and lowest BER values are shown in Fig.-8. According to eight different simulations of BPSK modulation, the lowest BER value was taken at 0 SNR in two channels, and the highest BER value was 30 dB in one channel.

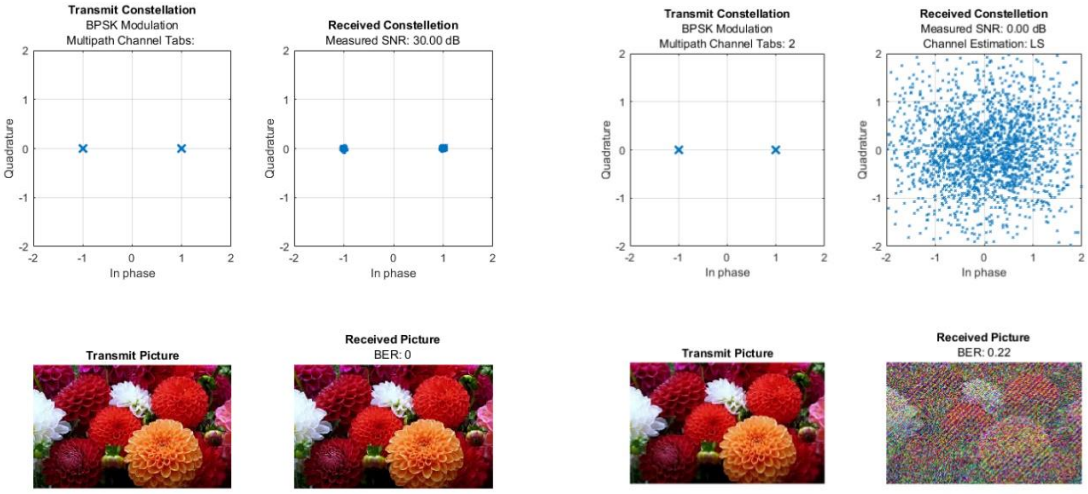

Figure 8. BPSK modulation highest and lowest BER values

5.2. QPSK Modulation

QPSK provides four different outputs for a single carrier frequency. Four different input states must occur for these four different output phases. For four different input combinations to happen in the QPSK modulator, the input signal of the QPSK modulator must be in the form of a digital binary system [14]. With the two bits to be given to the input, four different states are created as 00,01,10,11. The same variables as in BPSK were tried in the simulation, respectively, and the highest and lowest BER values were shown in Fig. 9.

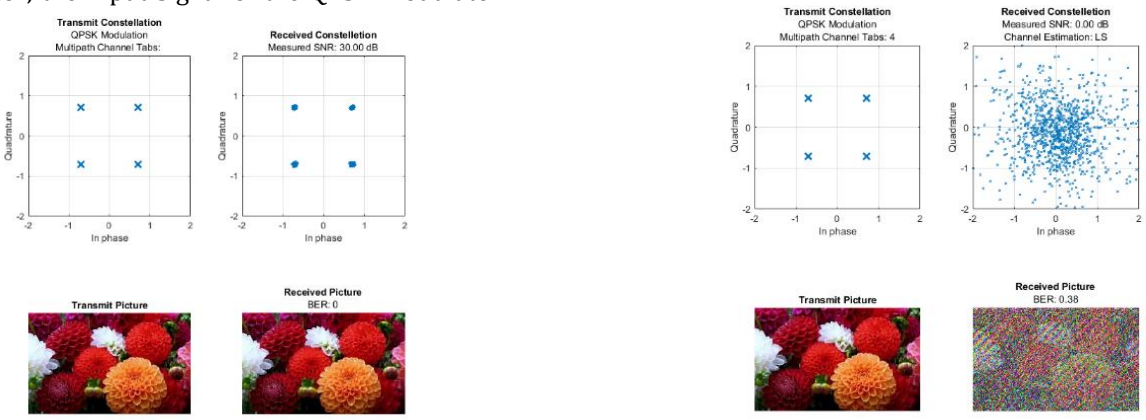

Figure 9. QPSK modulation highest and lowest BER values

5.3. 8PSK modulation

In 8PSK, eight possible states of three consecutive bits are assigned to a carrier signal's eight specified phase positions. Three bits are moved with each phase change. Phase changes are 0, 45, 90, 135, 180, 225, 270 and 315 degrees [21] . The same variables as in QPSK were tried in the simulation, respectively, and the highest and lowest BER values were shown in Fig. 10.

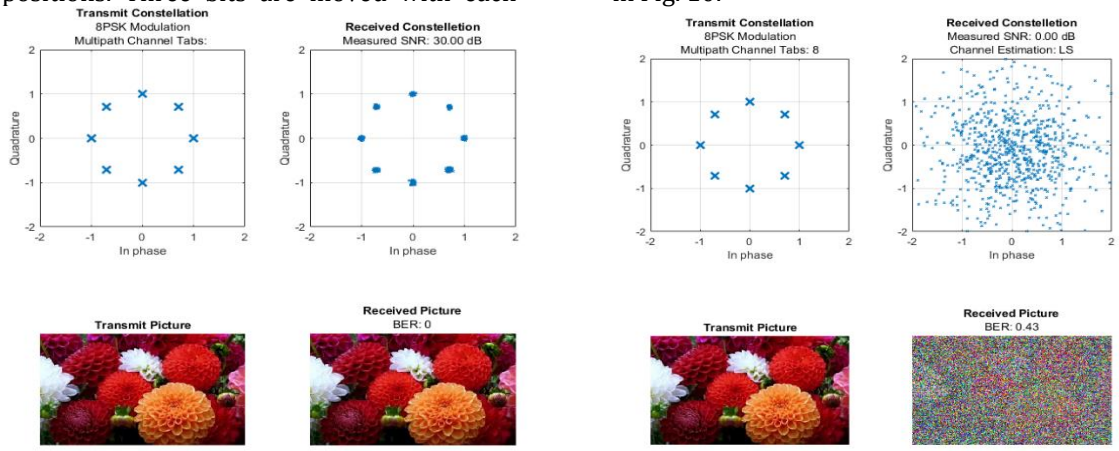

Figure. 10. 8PSK modulation highest and lowest BER values

5.4. 16-QAM Modulation

16-QAM provides 16 different outputs for a single carrier frequency. For these 16 different outputs, 16 different input states must occur. For different input combinations to occur in the 16-QAM modulator, the input signal of the 16-QAM modulator must be in the form of 4 digital bits [22]. The same variables as in 8PSK were tried in the simulation, respectively, and the highest and lowest BER values were shown in Fig. 11.

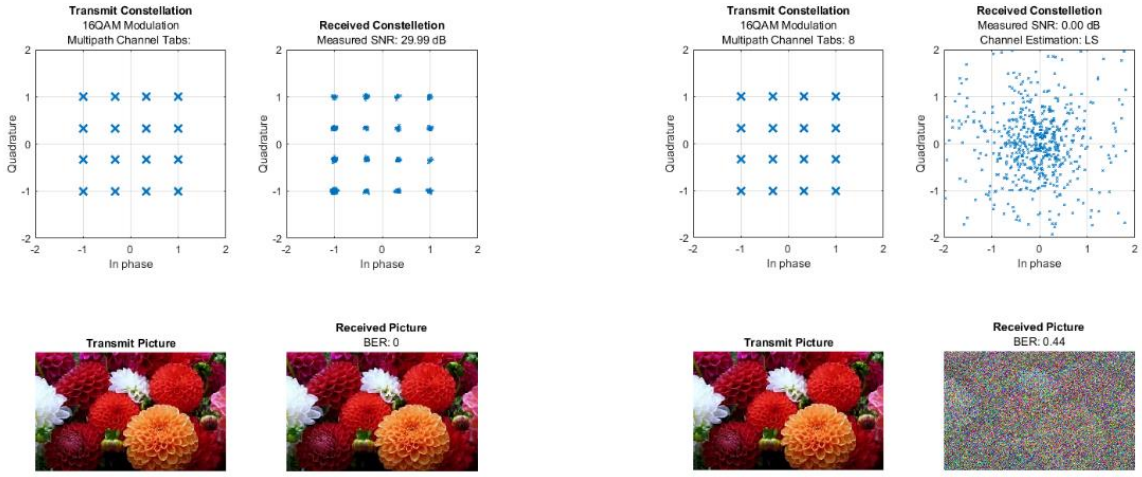

Figure 11. 16 QAM modulation highest and lowest BER values

5.5. 32-QAM Modulation

32-QAM provides 32 different outputs for a single carrier frequency. For these 32 different outputs, 16 different input states must occur. For different input combinations to occur in the 32-QAM modulator, the input signal of the 32-QAM modulator must be in the form of 5 digital bits [23]. In the simulation, the same variables as in the 16-QAM modulation were tried, respectively, and the highest and lowest BER values are shown in Fig. 12.

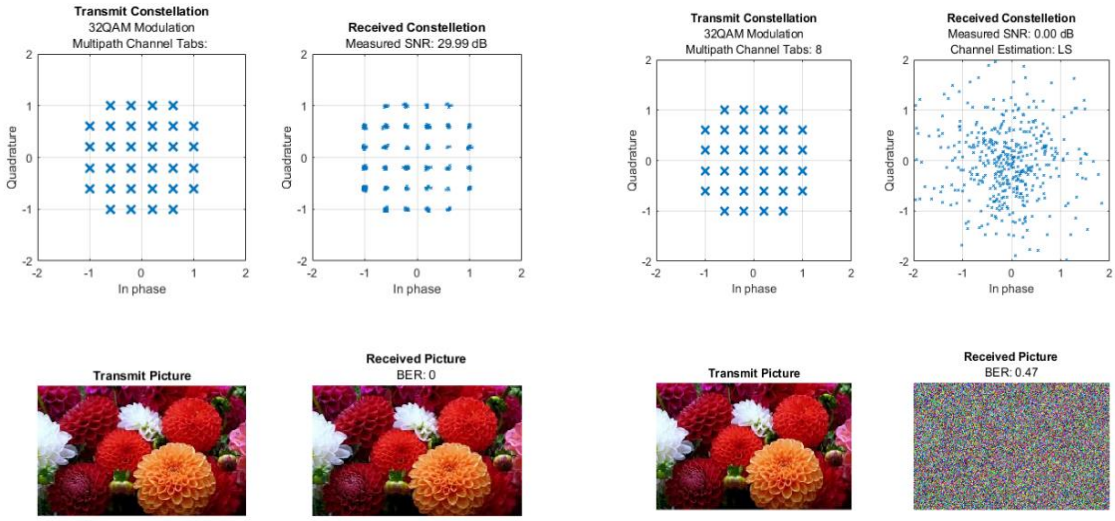

Figure 12. 32 QAM modulation highest and lowest BER values

5.6. 64-QAM Modulation

64-QAM provides 64 different outputs for a single carrier frequency. For these 64 different outputs to occur, 64 different input states must occur. For different input combinations to occur in the 64-QAM modulator, the input signal of the 64-QAM modulator must be in the form of 6 bits [24]. The same variables were tried in the simulation as in 32-QAM modulation, respectively, and the highest and lowest BER values are shown in Fig. 13.

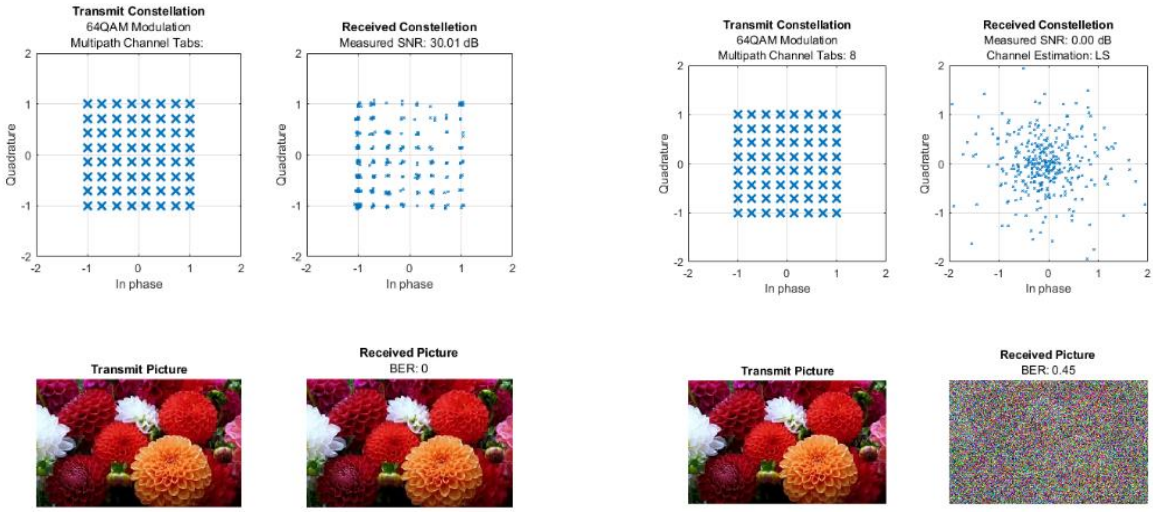

Figure 13. 64QAM modulation highest and lowest BER values

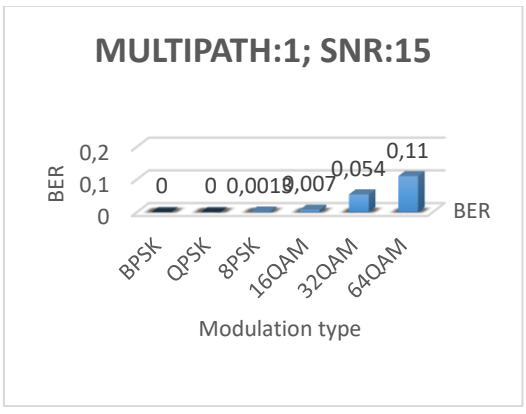

Figure 14. BER ratios for single-channel and signal-to-noise ratio of 15dB

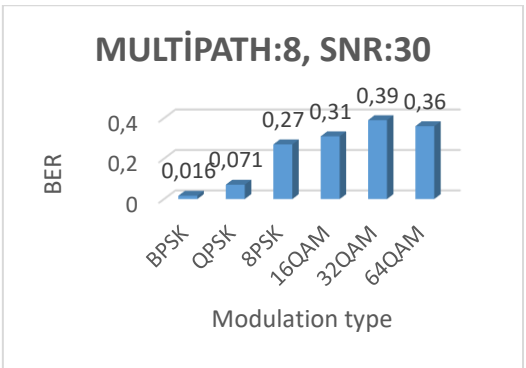

Figure 15. BPSK is the modulation type with the most successful BER rate in all simulation situations

6. Conclusions

The study proved the necessity of an OFDM system by simulating the transmission of multiple information signals from a single channel as FDM with a coherent structure. Here, reducing bandwidth in band-modulated data transmission is the most significant advantage of the OFDM system. The study compared the types of modulation used in OFDM communication.

As a result of seventy-two (72) simulations, it was observed that there was no change in the BER values of 30 dB and beyond and that the BER ratio was 0 in all modulation types when the multi-channel was single and the SNR ratio was 30 dB. Therefore, it is seen in Fig.-14 that PSK modulation is more successful against noise than other QAM modulations in all modulation types. Furthermore, BPSK modulation has been the most successful BER ratio among all modulation types in PSK modulation, as seen in Fig.-15. Therefore, when speed and error rate are considered, BPSK and QPSK modulation is the most commonly used modulation type in OFDM communication

Acknowledgement

This work was supported by the Scientific Research Projects Unit of Duzce University under project number 2021.06.01.1204. The authors appreciate the financial and scientific support.

References

[1] Kumar S, Payal, Enhancing Performance of Coherent Optical OFDM FSO Communication Link Using Cascaded EDFA, Wirel. Pers. Commun., no. 0123456789, 2021, DOI: 10.1007/s11277-021-08506-z.

[2] Zhou J, Yu J, Cheng Q, Shi J, Guo M, Tang X, Qiao Y. 256-QAM Interleaved Single Carrier FDM for Short-Reach Optical Interconnects, IEEE Photonics Technol. Letters, 29(21), 1796–1799, 2017. DOI: 10.1109/LPT.2017.2752215.

[3] Elango K, Muniandi K, VLSI implementation of an area and energy-efficient FFT/IFFT core for MIMO-OFDM applications, Ann. des Telecommun. Telecommun., 75(5–6), 215–227, 2020. DOI: 10.1007/s12243-019-00742-6.

[4] Balaji KA,. Prabu K. BER analysis of relay assisted PSK with OFDM ROFSO system over Malaga distribution including pointing errors under various weather conditions, Opt. Commun., vol. 426, no. May, pp. 187–193, 2018, DOI: 10.1016/j.optcom.2018.05.027.

[5] Hema R, Sudha S, Aarthi K. Performance studies of MIMO based DCO-OFDM in underwater wireless optical communication systems, Journal of Marine Science and Technology (Japan), 26(1), 97–107, 2021. DOI: 10.1007/s00773-020-00724-7.

[6] Jung WS, Lim KW, Ko YB. Utilising partially overlapped channels for OFDM-based 802.11 WLANs, Comput. Commun., 63(1), 77–86, 2015. DOI: 10.1016/j.comcom.2015.02.013.

[7] Barneto CB, Riihonen T, Turunen M, Anttila L, Fleischer M, Stadius K, Ryynänen J, Valkama M. Full-Duplex OFDM Radar with LTE and 5G NR Waveforms: Challenges, Solutions, and Measurements, IEEE Trans. Microw. Theory Tech., 67(10), 4042–4054, 2019. DOI: 10.1109/TMTT.2019.2930510.

[8] Penagos HP. OFDM comparison with FFT and DWT processing for DVB-T2 wireless channels, Inge Cuc, 14(2), 97–105, 2018. DOI: 10.17981/ingecuc.14.2.2018.09.

[9] Al-Dweik A, Xiong F. Frequency-hopped multiple-access communications with noncoherent M-ary OFDM-ASK, IEEE Trans. Commun., 51(1), 33–36, 2003. DOI: 10.1109/TCOMM.2002.807620.

[10] Marti J, Capmany J. Laser Linewidth Impairment on Thean Performance of OFDM-FSK Systems Employing Single-Cavity Fabry-Perot Demultiplexers, IEEE Photonics Technol. Lett., 7(5), 561–563, 1995. DOI: 10.1109/68.384544.

[11] Huh H, Lu F, Krogmeier JV. Exact intersymbol interference analysis for upsampled OFDM signals with symbol timing errors, IEICE Trans. Commun., E100B(8), 1472–1479, 2017. DOI: 10.1587/transcom.2016EBP3433.

[12] Ertürk S. Sayısal Haberlesme. Birsen Yayınevi 2005.

[13] Sharma S, Gupta R. Performance Comparison of OFDM System with Different Modulation Methods, Commun. Appl. Electron., 5(2), 18–21, 2016. DOI: 10.5120/cae2016652222.

[14] Le ST, McCarthy ME, Suibhne NM, Giacoumidis E, Doran NJ, Ellis AD. Comparison of bit error rate estimation methods for QPSK CO-OFDM transmission, IEEE Photonics Technol. Letters, 26(22), 2244–2247, 2014. DOI: 10.1109/LPT.2014.2352460.

[15] Hoxha J, Shimizu S, Cincotti G. On the performance of all-optical OFDM based PM-QPSK and PM-16QAM, Telecommun. Syst., 75(4), 355–367, 2020. DOI: 10.1007/s11235-020-00687-5.

[16] Peng B, Wang X, Brink ST. On Receive Window Design for UF-OFDM Signals over Multipath Channels, IEEE Commun. Letters, 24(10), 2349–2352, 2020. DOI: 10.1109/LCOMM.2020.3005996.

[17] Mohammed S. Orthogonal Frequency Division Multiplexing (OFDM). https://www.slideshare.net/shoaybmohammed/orthogonal-frequency-division-multiplexing-ofdm-69596792 (Accessed: May 16, 2021).

[18] Kamal S, Kang H, Meza CAA, Kim DS. Improved dual sync pulses to reduce ICI power and PAPR in OFDM-based systems, KSII Trans. Internet Inf. Syst., 14(12), 4930–4948, 2020. doi: 10.3837/tiis.2020.12.017.

[19] Street J, ofdm_sim. https://www.mathworks.com/matlabcentral/m

lc-downloads/downloads/submissions/67156/versions/1/previews/OFDM_Channel_Estimation/html/ofdm_sim.html (Accessed: Apr. 26, 2021).

[20] Bolaji AG, Shongwe T. Performance comparison of modified BPSK-OFDM and QFSK-OFDM in PLC channel noise, Int. J. Electron. Telecommun., 66(4), 499–605, 2020. doi: 10.24425-ijet.2020.134017/740.

[21] Kareem AHA. Performance evaluation of PSK all optical OFDM system based on arrayed waveguide grating under different weather conditions, Int. J. Microw. Opt. Technol., 15(1), 85–94, 2020.

[22] Xiang C, Yang X, Zhou X, Zhu X, Xu J, He Q. Improved Training Sequence Channel Estimation Scheme in 16QAM MB-OFDM UWBoF System, Adv. Condens. Matter Phys., 2020(6273892), 2020. doi: 10.1155/2020/6273892.

[23] Huang MF, Zhang S, Mateo E, Qian D, Yaman F, Inoue T. EDFA-only WDM 4200-km transmission of OFDM-16QAM and 32QAM, IEEE Photonics Technol. Letters, 24(17), 1466–1468, 2012. doi: 10.1109/LPT.2012.2205378.

[24] Zhou Z, Liu L, Wang G. 2.03 Gbps visible light communication system with 64-QAM-OFDM utilizing a single flip-chip blue GaN-LED, J. Mod. Opt., 66(21), 2114–2118, 2019. doi: 10.1080/09500340.2019.1695974.

[25] Louis E, Frenzel JR. Principles of Electronic Communication Systems,28(10), 2015.

Uluslararası Teknolojik Bilimler Dergisi
International Journal of Technological Sciences
UTBD
IJTS

Research Article/Araştırma Makalesi

Investigation of the effects of seasonal temperatures on ammonia-water absorption heat pumps for Isparta province

Ahmet Elbir[*1]

[1]Süleyman Demirel University, YEKARUM, 32260, Isparta, Türkiye

Keywords
Ammonia-water absorption
Heat pump
COP
Climatic conditions
Energy efficiency

Article history:
Received: 03.10.2024
Accepted: 09.12.2024

Abstract: This study analyzes the performance of ammonia-water absorption heat pump systems for Isparta province. Considering the variable climate conditions of Isparta, the effects of seasonal temperatures on heat pump performance were investigated. In the study, it was observed that the ammonia-water absorption heat pump showed acceptable performance even at low outdoor temperatures, and the efficiency of the system increased as the temperature increased. While the COP (coefficient of performance) values were 0.7981 in January, they increased to 0.8138 in September. These results reveal that ammonia-water absorption heat pumps offer a suitable solution in terms of energy efficiency in regions with climatic differences such as Isparta. In addition, when compared with the studies in the literature, it is seen that this system provides reasonable efficiency at low temperatures. The general findings of the study show that ammonia-water absorption heat pumps provide reasonable performance at low temperatures, but operate more efficiently at high temperatures. In this context, it was concluded that these systems are a suitable option in terms of energy efficiency in regions with high seasonal temperature changes, such as Isparta.

To Cite/Atıf için: Elbir A. Investigation of the effects of seasonal temperatures on ammonia-water absorption heat pumps for Isparta province. International Journal of Technological Sciences, 16(2), 44-52, 2024.

Isparta ili için amonyak-su absorpsiyonlu ısı pompaları üzerindeki mevsimsel sıcaklıkların etkilerinin araştırılması

Anahtar Kelimeler
Amonyak-su absorpsiyon
Isı pompası
COP
İklim koşulları
Enerji verimliliği

Makale geçmişi:
Geliş Tarihi: 03.10.2024
Kabul Tarihi: 09.12.2024

Öz: Bu çalışma, Isparta ili için amonyak-su absorpsiyon ısı pompası sistemlerinin performansını analiz etmektedir. Isparta'nın değişken iklim koşulları dikkate alınarak, mevsimsel sıcaklıkların ısı pompası performansı üzerindeki etkileri incelenmiştir. Çalışmada, amonyak-su absorpsiyon ısı pompasının düşük dış ortam sıcaklıklarında dahi kabul edilebilir bir performans gösterdiği, sıcaklık arttıkça ise sistemin verimliliğinin arttığı gözlemlenmiştir. COP (performans katsayısı) değerleri Ocak ayında 0.7981 iken, Eylül ayında 0.8138'e kadar yükselmiştir. Bu sonuçlar, amonyak-su absorpsiyon ısı pompalarının Isparta gibi iklimsel farklılıklar gösteren bölgelerde enerji verimliliği açısından uygun bir çözüm sunduğunu ortaya koymaktadır. Ayrıca, literatürdeki çalışmalarla karşılaştırıldığında, bu sistemin düşük sıcaklıklarda da makul bir verimlilik sağladığı görülmektedir. Çalışmanın genel bulguları, amonyak-su absorpsiyon ısı pompalarının düşük sıcaklıklarda makul bir performans sunduğunu, ancak yüksek sıcaklıklarda daha verimli çalıştığını ortaya koymaktadır. Bu bağlamda, Isparta gibi mevsimsel sıcaklık değişikliklerinin yüksek olduğu bölgelerde bu sistemlerin enerji verimliliği açısından uygun bir seçenek olduğu sonucuna varılmıştır.

* İlgili yazar/Corresponding author: ahmetelbir@sdu.edu.tr

1. Introduction

Isparta is an important city located in the Mediterranean Region of Turkey. The climate conditions of the region are hot and dry in summers and cold and rainy in winters. These climate characteristics are important factors that determine the heating and hot water needs of the local population and industry. In this context, it is important to research alternative heating and hot water systems in terms of energy efficiency and environmental sustainability. Ammonia-water absorption heat pumps are a technology that uses environmentally friendly refrigerants such as ammonia and water to transfer thermal energy. These systems provide high efficiency while minimizing the impact on the environment by reducing electrical energy use. Compared to traditional heat pumps, ammonia-water absorption heat pumps offer lower operating costs and longer life. Potential application areas of ammonia-water absorption heat pumps for Isparta include:

• Residential Heating and Hot Water Systems: Heat pumps supported by solar energy in the summer months can be used to provide hot water and heating in residences. In winter months, ammonia-water absorption heat pumps can operate effectively despite low outdoor temperatures.

• Industrial Process Heating: Isparta province is home to important industries such as agriculture and textile. It is possible to make the process heating systems used in these industries more efficient with ammonia-water absorption heat pumps.

• Greenhouse and Agricultural Heating: Greenhouse farming is of great importance in Isparta's agricultural production. Ammonia-water absorption heat pumps can be a suitable solution for controlling the temperature inside the greenhouse and growing agricultural products.

In this context, it is recommended that the use of ammonia-water absorption heat pumps be encouraged and supported locally for Isparta province. Evaluating the performance of the ammonia-water absorption heat pump system according to the outdoor temperature of Isparta will make your article more comprehensive and suitable for the local context. The originality of the study is that there are limited studies on the performance of ammonia-water absorption heat pumps in regions with intense seasonal temperature changes, such as Isparta. Your study is important in terms of providing energy efficiency solutions suitable for local climate conditions.

2. Literature Review

This study performed energy and exercise analysis of an ammonia-water absorption refrigeration system (AWARS) for domestic solar cooling systems. The study found that the COP value was 0.7 when the evaporator temperature was 5 °C and the condenser temperature was 30 °C [1]. Modeling and experimental analysis of GAX NH3–H2O gas powered absorption heat pump were performed. The experimental results show that the COP value was 1.2 when the evaporator temperature was 15 °C and the condenser temperature was 40 °C [2]. Performed seasonal performance evaluation of three alternative gas-powered absorption heat pump cycles. In the study, the highest COP value of the system was determined as 1.5; the evaporator temperature is 10 °C and the condenser temperature is 35 °C [3]. This book discusses the applications of thermal energy storage systems and the integration of NH_3-H_2O systems. The book determined the temperatures at which NH_3-H_2O systems operate at their highest efficiency as 5 °C and 45 °C [4]. The start-up time of aqua-ammonia and water-lithium bromide absorption chiller systems under different heat exchanger configurations was compared. The results show that the COP value is 0.9 for aqua-ammonia and 1.2 for water-lithium bromide at an evaporator temperature of 10 °C and a condenser temperature of 35 °C [5]. Simulation and comparison of NH_3-H_2O absorption cycles were performed. The study determined that the COP value of the system is 1.1 when the condenser temperature is 30 °C and the evaporator temperature is 10 °C [6]. An environmental life cycle assessment was conducted between a condensing boiler and a gas-fired absorption heat pump. The obtained data show that the absorbers temperature is 25 °C and the COP value is 0.95 [7]. A study was conducted on monitoring and comparing the primary energy efficiency of gas-fired absorption heat pumps. In the study, the evaporator temperature was determined as 5 °C and the condenser temperature was 30 °C; under these conditions, the COP value was measured as 0.85 [8]. The performance characteristics of the NH_3-H_2O absorption heat pump system were investigated. In the study, the COP value was determined as 1.2 under conditions where the evaporator temperature was 10 °C and the condenser temperature was 35 °C [9]. Simulation and performance analysis of an NH_3-H_2O absorption heat pump based on generator-absorber heat exchange (GAX) cycle was performed. The results

showed that the COP value was 0.88 when the evaporator temperature was 0 °C and the condenser temperature was 40 °C [10]. Performance comparison of NH_3-H_2O and water-lithium bromide solutions in vapor absorption refrigeration systems was performed. In the study, the evaporator temperature was determined as 10 °C and the COP value was 1.0 for the NH_3-H_2O system [11]. NH_3-H_2O hybrid absorption-compression heat pump for heat supply in a spray-drying facility was optimized using exergoeconomic analysis. The results showed a COP of 1.3 with evaporator and absorber temperatures of 10 °C and 30 °C, respectively [12]. Large capacity NH_3-H_2O and water-lithium bromide vapor absorption refrigeration cycles were compared. Results indicated a COP of 1.1 for NH_3-H_2O at an evaporator temperature of 5 °C and a condenser temperature of 30 °C [13]. Comparison of NH_3-H_2O and water-lithium bromide solutions in absorption heat transformers was carried out. The study revealed that the COP value of the NH_3-H_2O system at an evaporator temperature of 10 °C was 1.0 [14]. An experimental investigation was carried out on the NH_3-H_2O absorption cycle for transporting heat over long distances. In this study, the performance of the system was found to be 0.95 with a COP value at 0 °C evaporator and 40 °C condenser temperatures [15]. Experimental results for heat recovery of NH_3-H_2O system in industrial processes present a COP value of 1.1 at 0 °C evaporator temperature and 35 °C condenser temperature [16]. Design and analysis of NH_3-H_2O absorption heat pump were carried out. In the study, the COP value was measured as 1.0 for 10 °C evaporator temperature and 30 °C condenser temperature [17]. First law thermodynamic evaluation of NH_3-H_2O absorption heat pump systems was carried out. The obtained results determined the COP value as 0.9 at 10 °C evaporator temperature and 35 °C condenser temperature [18]. Performance improvement of gas-fired absorption heat pumps by controlling the flow rate. The study shows that the COP value is 1.2 at 15 °C evaporator temperature and 40 °C condenser temperature [19]. An experimental investigation was carried out on ammonia-water-lithium bromide absorption refrigeration system without a solution pump. In the study, the performance of the system presents a COP value of 0.95 at 10 °C evaporator temperature and 35 °C condenser temperature [20]. Performance evaluation of small-scale (AWARS) was conducted. In the study, the COP value was measured as 1.1 at 15 °C evaporator temperature and 40 °C condenser temperature [21]. Simulation analysis was carried out on the performance optimization of gas-fired NH_3-H_2O absorption heat pump. In the study, a COP value of 1.0 was determined at 10 °C evaporator temperature and 30 °C condenser temperature [22]. Experimental analysis of a “thermally driven” solution pump using a small capacity NH_3-H_2O absorption heat pump was carried out. The study achieved a COP of 0.8 at an evaporator temperature of 5 °C [23].

3. Materials and methods

3.1. Climatic conditions of Isparta

Isparta's climate conditions are characterized by high temperatures in summer and low temperatures in winter. This can directly affect the performance of the NH_3-H_2O absorption heat pump system. Especially in winter, low outdoor temperatures can reduce the efficiency of the system. The analyses show that when the outdoor temperature drops below 0°C, the COP value of the system decreases significantly. In summer, increasing temperatures allow the system to operate more effectively. In this context, optimizations and system design recommendations suitable for Isparta's climate conditions are presented. In addition, simulations evaluating the effects of different temperature scenarios on performance provide important findings for local energy efficiency applications.

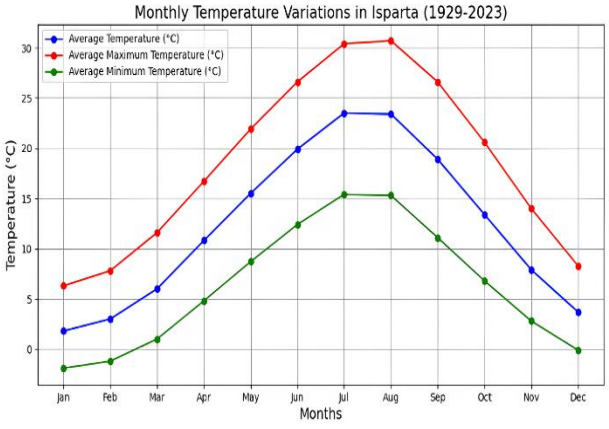

Figure 1. Isparta monthly temperature change [24]

General Directorate of Meteorology [GDM] This institution provides Turkey's official meteorological data. Isparta's annual temperature averages and seasonal changes are given in Figure 1.

3.2. Working diagram of the absorption system

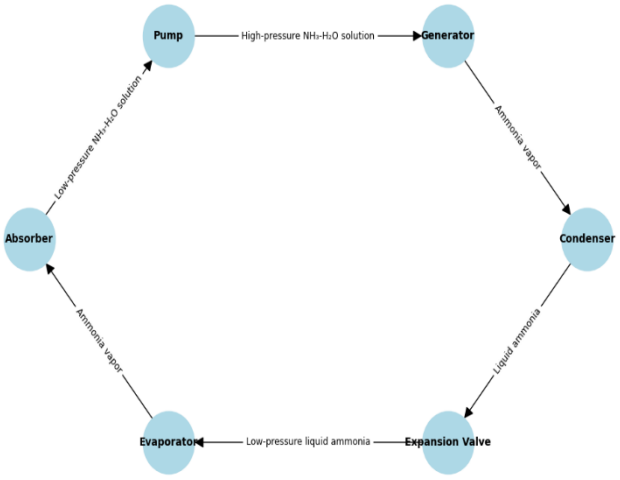

Figure 2. Ammonia water heat pump flow diagram

Figure 2 shows a thermal system that uses a mixture of ammonia (NH_3) and water (H_2O) as an alternative to a vapor compression cycle. The operating principle of this system is based on taking heat from one medium and transferring it to another medium, but here an absorption and desorption process is used instead of a compressor. The basic operating principle of the NH_3-H_2O absorption heat pump is explained step by step below: The NH_3-H_2O mixture comes into play at this point. While the ammonia is operating in the low-pressure side of the system in the vapor phase, this vapor is absorbed by the water and an NH_3-H_2O solution is obtained. During this process, heat is taken from the environment, which performs the cooling or heating function of the system. The absorbed NH_3-H_2O solution is transported from low pressure to high pressure. This is done with a mechanical pump that consumes very little energy. The solution, which is brought to high pressure, is then sent to the generator. Heat is added to the NH_3-H_2O solution under high pressure. This heat energy is usually provided by a boiler or a source such as solar energy. During this process, ammonia is separated from the water solution and ammonia vapor emerges. Water remains in the generator. The ammonia vapor leaving the generator goes to the condenser. Here, the vapor is condensed with the help of cooling water or air and turned into liquid. During condensation, ammonia vapor releases heat to the environment. This stage is when the system operates in heating mode. The condensed liquid ammonia is sent to the evaporator by reducing its pressure through the expansion valve. In the meantime, the pressure and temperature of the ammonia decrease. The low-pressure ammonia liquid evaporates again by taking heat from the environment in the evaporator. The ammonia vapor absorbs heat from the low-temperature environment and cools the environment. During this process, the vapor performs the cooling process of the evaporator by absorbing the heat from the environment. The vaporized ammonia returns to the absorber and the cycle starts again. In this system, a heat source is used instead of a compressor and the absorption/desorption processes of the water-ammonia solution take place. NH_3-H_2O absorption heat pumps offer an efficient heating and cooling solution with low energy consumption and are more environmentally friendly than fossil fuel systems.

3.3. Comparison with Other Energy Systems

NH_3-H_2O absorption heat pumps offer an important option in terms of energy efficiency and environmental sustainability. However, when compared to different heating and cooling systems, a detailed analysis is required to determine which system is more advantageous. Below is an evaluation comparing the NH_3-H_2O absorption heat pump with other energy systems (such as electric heat pumps and fossil fuel systems).

Electric heat pumps are systems that transfer heat from the air or ground to the interior. They perform cooling or heating processes using electrical energy. Their COP values usually range from 3 to 4, meaning they produce 3 to 4 units of heat for each unit of electrical energy. They are compatible with high efficiency, low operating costs and environmentally friendly energy sources. The high electricity costs and the reduced efficiency of electric heat pumps in some regions reduce their effectiveness in the winter months when the outdoor temperature is low.

Fossil fuel systems generate heat using fuels such as natural gas, diesel or coal. Generally, these systems generate energy through combustion. They usually offer efficiency between 70-90%; but this varies depending on the type of fuel used and the type of system. Low initial costs and high heat generation capacity. Carbon emissions and environmental impacts, depletion of fossil fuels, fluctuating fuel costs.

3.4. Thermodynamic calculations and their assumption

The thermodynamic analysis was made with the EES software (Engineering Equation Solver) [25]. Since the NH_3-H_2O absorption heat pump is a thermal system, the COP value is calculated by the formula:

$$COP=\frac{\text{Cooling or Heating Power Generated}}{Energy\ Used\ in\ Input\ (Heat)} \quad [1]$$

This system absorbs heat at low temperature in the evaporator and receives energy from a heat source. COP values typically depend on temperature differences and the properties of the fluid used in the system. When calculating COP values at different temperatures:

• Evaporator temperature (low temperature) is the part where absorption occurs.
• Condenser temperature (high temperature) is the condensing temperature.
• COP varies depending on the efficiency of the heat energy at the inlet and the behavior of the fluid in the cycle.
Absorption systems at low temperatures usually have lower COP values because the temperature difference between the evaporation and condensation processes is small.

Electric heat pumps transfer heat from the external environment using a mechanical cycle. COP is usually calculated as follows:

$$COP=\frac{\text{Transferred Heat}}{Electrical\ Energy\ Consumed} \quad [2]$$

The COP value changes depending on the outside temperature. As the outside temperature increases, the COP value of an electric heat pump increases because the system works more efficiently as the temperature difference decreases. Electric heat pumps use the heat they receive from the outside environment to heat or cool, and therefore their efficiency increases as the ambient temperature increases.

Fossil fuel systems usually work with a boiler or combustion system. Efficiency is calculated with the following formula:

$$\text{Efficiency}(\%)=\frac{Output\ Power\ (Heat\ or\ Energy)}{Input\ Energy\ (Fuel\ Energy)}\text{X}100 \quad [3]$$

In fossil fuel systems, efficiency is calculated by factors such as combustion efficiency and boiler efficiency, and usually varies between 80% and 95%. These systems depend on the type of fuel and combustion efficiency rather than the outside temperature.

The values in the table are generally calculated using experimental data or standard COP and efficiency values in the literature. The operating performance of the relevant systems under temperature conditions has been determined by simulations. The general methods used for each system are summarized below:

• Absorption Heat Pump: COP values are calculated together with the evaporator, condenser and absorber temperatures. It is found using the cooling load and the thermal energy entering the system.
• Electric Heat Pump: COP is calculated based on the thermal energy transferred according to the electrical energy consumed.
• Fossil Fuel System: Efficiency is calculated by taking into account combustion efficiency and thermal losses.

As a result, the COP or efficiency value of each system is directly related to how the system operates and in which temperature range it is evaluated.

4. Findings

Table 1. Thermodynamic data of NH_3-H_2O absorption heat pump

Parameter	Value	Parameter	Value
T_evaporator [°C]	-5	Mass flow rate (m_dot) [kg/s]	0.05
P_evaporator [bar]	2	T_generator [°C]	120
x_evaporator	1	P_generator [bar]	10
T_condenser [°C]	35	Q_evaporator [kJ/s]	54.53
P_condenser [bar]	10	Q_generator [kJ/s]	68.32
x_condenser	0	COP	0.7981

Table 1 shows the thermodynamic data of the NH_3-H_2O absorption heat pump. The evaporator temperature (T_evaporator) was determined as -5°C, the evaporator pressure (P_evaporator) was 2 bar, and the steam quality at the evaporator outlet (x_evaporator) was determined as 1. The condenser temperature (T_condenser) was recorded as 35°C, the condenser pressure (P_condenser) as 10 bar and the steam quality

at the condenser outlet (x_condenser) as 0. The generator temperature (T_generator) is 120°C, the generator pressure (P_generator) is 10 bar, the mass flow rate (ṁ) is 0.05 kg/s, the amount of heat taken from the evaporator (Q_evaporator) is 54.53 kJ/s and the amount of heat taken from the generator (Q_generator) is 68.32 kJ/s. The performance coefficient (COP) of the system was calculated as 0.7981.

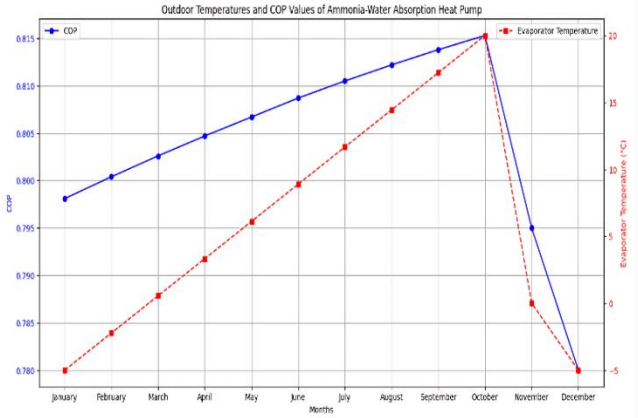

Figure 3. Effect of outdoor temperatures on COP in absorption system

Figure 3 shows the seasonal temperature data of the cooling system and the graphs showing the performance of an absorption heat pump. The data and detailed explanations of the graphs are given below: It represents 12 months of the year from January to December. It is the average outdoor temperature of a city located in a temperate climate zone like Turkey by month. For example, while the average temperature in January is 1.8°C, it is 23.5°C in July. The temperatures in the evaporator section of the absorption heat pump are calculated according to these data and outdoor temperatures. These temperatures vary between -5°C and 20°C. Lower values are seen in the winter months and higher values are seen in the summer months. It represents the coefficient of performance of the heat pump. The COP value varies between 0.7800 and 0.8153 and these values show the efficiency of the heat pump. The higher the COP, the more efficient the system is. The blue line shows the COP values by month in the graph. In January, the COP is 0.7981, while this value increases in the summer months, reaching 0.8138 in September, and then decreases again. The red dashed line shows the evaporator temperatures. This temperature starts at -5°C in January and increases in the summer months, reaching 17.22°C in September.

COP values vary seasonally. As outdoor temperatures increase in the summer months, the COP also tends to increase, indicating that the efficiency of the heat pump varies with the season. The evaporator temperature is directly related to the outdoor temperatures. As the ambient temperatures increase, the evaporator temperatures also increase. This graph can be used to analyze the seasonal performance of absorption heat pumps and helps us visually understand in which seasons the system is more efficient.

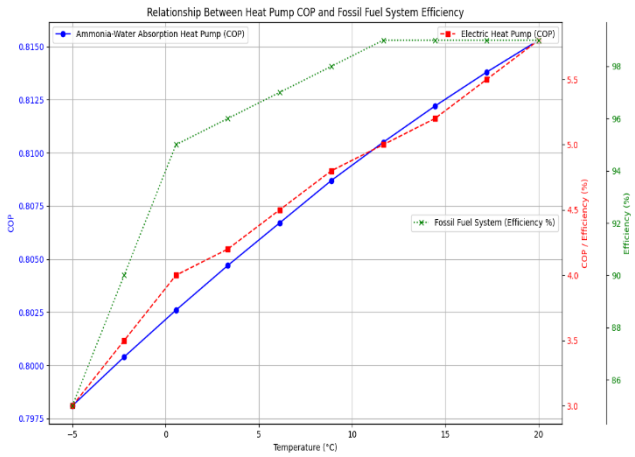

Figure 4. The relationship between heat pump COP and Fossil fuel system efficiency

Figure 4 investigates the coefficients of performance (COP) and efficiency of NH_3-H_2O absorption heat pump, electric heat pump and fossil fuel systems depending on certain temperature values. The numerical data used are summarized below: At temperature -5 °C, the COP of the NH_3-H_2O absorption heat pump is 0.7981, the COP of the electric heat pump is 3.0 and the efficiency of the fossil fuel system is 85%. At temperature -2.222 °C, the COP of the NH_3-H_2O absorption heat pump is 0.8004, the COP of the electric heat pump is 3.5 and the efficiency of the fossil fuel system has increased to 90%. At 0.5556 °C, the COP of the NH_3-H_2O absorption heat pump is 0.8026, the COP of the electric heat pump is 4.0 and the efficiency of the fossil fuel system is 95%. At 3,333 °C, the COP of the NH_3-H_2O absorption heat pump was 0.8047, the COP of the electric heat pump was 4.2, and the efficiency of the fossil fuel system was 96%. When the temperature was 6,111 °C, the COP of the NH_3-H_2O absorption heat pump was 0.8067, the COP of the electric heat pump was 4.5, and the efficiency of the fossil fuel system was 97%. At 8,889 °C, the COP of the NH_3-H_2O absorption heat pump was 0.8087, the COP of the electric heat pump was 4.8, and the efficiency of the

fossil fuel system was 98%. At 11.67 °C, the COP of the ammonia-water absorption heat pump was 0.8105, the COP of the electric heat pump was 5.0, and the efficiency of the fossil fuel system reached 99%. At 14.44 °C, the COP of the NH_3-H_2O absorption heat pump was 0.8122, the COP of the electric heat pump was 5.2, and the efficiency of the fossil fuel system was 99%. At 17.22 °C, the COP of the NH_3-H_2O absorption heat pump was 0.8138, the COP of the electric heat pump was 5.5, and the efficiency of the fossil fuel system was 99%. Finally, at 20 °C, the COP of the NH_3-H_2O absorption heat pump was 0.8153, the COP of the electric heat pump was 5.8, and the efficiency of the fossil fuel system reached 99%. The obtained data show that as the temperature increases, the COP of the NH_3-H_2O absorption heat pump increases from 0.7981 to 0.8153, and the COP of the electric heat pump ranges from 3.0 to 5.8. In addition, the efficiency of the fossil fuel system increases from 85% to 99%. These numerical data clearly show the temperature-dependent performance of each system and enable comparisons between energy systems.

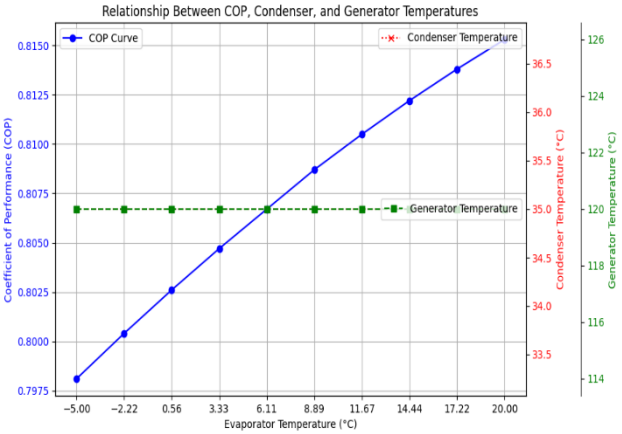

Figure 5. Relationship between COP, condenser temperature, evaporator temperature and generator temperature

Figure 5 visualizes the relationship between Coefficient of Performance (COP), condenser temperature, evaporator temperature, and generator temperature. The data is organized in a dictionary format that includes: A set of coefficients of performance ranging from 0.7981 to 0.8153. A fixed temperature for the condenser of 35 °C. A set of evaporator temperatures ranging from -5 °C to 20 °C. A fixed generator temperature of 120 °C. A blue line and circular markers for COP. A red dotted line and x markers for condenser temperature. A green dashed line and square markers for generator temperature. The graph is appropriately labeled, with axis labels and a title. There is also a legend indicating which line corresponds to which parameter. The grid feature is enabled and the graph size is set to 10 x 6 inches for improved readability. This visualization helps to understand how COP varies with changes in evaporator temperature, together with fixed condenser and generator temperatures. The obtained COP values generally show similar performance when compared to the studies in the literature, but there are some differences. For example, in January, when the outdoor temperature is 1.8°C and the evaporator temperature is -5°C, the COP value is calculated as 0.7981. This value is higher than the COP value of 0.7 obtained in the study of Aman et al. (2014) when the evaporator temperature is 5°C and the condenser temperature is 30°C. This situation shows that the NH_3-H_2O absorption heat pump in your study offers acceptable performance even at low temperatures. In the summer, in July, when the outdoor temperature is 23.5°C and the evaporator temperature is 11.67°C, the COP value is found as 0.8105. This result is similar to the COP value of 0.8105 obtained in the study of Aprile et al. (2016) study, it is lower than the COP value of 1.2 obtained at 15°C evaporator temperature and 40°C condenser temperature. This difference shows that condenser temperatures have a significant effect on system performance. In addition, in the study of Dehghan et al. (2020), the highest COP value of the gas-fired absorption heat pump system was determined as 1.5 when the evaporator temperature was 10°C and the condenser temperature was 35°C. It is quite high compared to the highest COP value of 0.8138 obtained in this article. This difference may be due to the different characteristics of the systems used and indicates that additional studies should be conducted for the optimization of the system.

In general, the ammonia-water absorption heat pump system exhibits competitive performance compared to other studies in the literature at low temperatures, but the COP values at high temperatures are slightly lower compared to the literature.

5. Conclusions

In this study conducted for Isparta province, the performance of the ammonia-water absorption heat pump was analyzed depending on the outdoor temperatures. The effect of seasonal temperature

changes on the system efficiency was examined through coefficient of performance (COP) and evaporator temperatures.

In January, when the outdoor temperature was 1.8°C, the evaporator temperature was determined as -5°C and the system COP value was measured as 0.7981. In the summer months, especially in July, the outdoor temperature increased to 23.5°C, while the evaporator temperature reached 11.67°C and the system COP value increased to 0.8105. The highest efficiency was seen in September, when the outdoor temperature was 18.9°C, the COP value was recorded as 0.8138.

These data show that the ammonia-water absorption heat pump operates with lower efficiency at low temperatures, but the system performance improves significantly as the temperature increases. It was observed that the system operates more efficiently, especially in the summer months. As a result, ammonia-water absorption heat pumps were evaluated as a heating solution suitable for the variable climatic conditions of Isparta and were shown to have significant potential in terms of local energy efficiency.

References

[1] Aman J, Ting DK, Henshaw P. Residential solar air conditioning: Energy and exergy analyses of an ammonia–water absorption cooling system. Applied Thermal Engineering, 62(2), 424-432, 2014.

[2] Aprile M, Scoccia R, Toppi T, Guerra M, Motta M. Modelling and experimental analysis of a GAX NH3–H2O gas-driven absorption heat pump. International Journal of Refrigeration, 66, 145-155, 2016.

[3] Dehghan B, Toppi T, Aprile M, Motta M. Seasonal performance assessment of three alternative gas-driven absorption heat pump cycles. Journal of Building Engineering, 31, 101434, 2020.

[4] Din I, Rosen MA. Thermal energy storage: systems and applications. John Wiley & Sons, 2011.

[5] Ebrahimnataj Tiji A, Ramiar A, Ebrahimnataj M. Comparison the start-up time of the key parameters of aqua-ammonia and water–lithium bromide absorption chiller (AC) under different heat exchanger configurations. SN Applied Sciences, 2, 1-14, 2020.

[6] Engler M, Grossman G, Hellmann HM. Comparative simulation and investigation of ammonia-water: absorption cycles for heat pump applications. International Journal of Refrigeration, 20(7), 504-516, 1997.

[7] Famiglietti J, Toppi T, Pistocchini L, Scoccia R, Motta M. A comparative environmental life cycle assessment between a condensing boiler and a gas driven absorption heat pump. Science of the Total Environment, 762, 144392, 2021.

[8] Fumagalli M, Sivieri A, Aprile M, Motta M, Zanchi M. Monitoring of gas driven absorption heat pumps and comparing energy efficiency on primary energy. Renewable Energy, 110, 115-125, 2017.

[9] Gadalla MA, Ibrahim TA, Hassan MA. Performance characteristics of an ammonia–water absorption heat pump system. International Journal of Energy Research, 37(14), 1917-1927, 2013.

[10] Grossman G, DeVault RC, Creswick FA. Simulation and performance analysis of an ammonia-water absorption heat pump based on the generator-absorber heat exchange (GAX) cycle. Oak Ridge National Lab., 1995.

[11] Horuz I. A comparison between ammonia-water and water-lithium bromide solutions in vapor absorption refrigeration systems. International Communications in Heat and Mass Transfer, 25(5), 711-721, 1998.

[12] Jensen JK, Markussen WB, Reinholdt L, Elmegaard B. Exergoeconomic optimization of an ammonia–water hybrid absorption–compression heat pump for heat supply in a spray-drying facility. International Journal of Energy and Environmental Engineering, 6, 195-211, 2015.

[13] Khan MS, Kadam ST, Kyriakides AS, Hassan I, Papadopoulos AI, Rahman MA, Seferlis P. Comparative Energy and Exergy Analysis of Large Capacity Ammonia-Water and Water-Lithium Bromide Vapor Absorption Refrigeration (VAR) Cycles. ASME International Mechanical Engineering Congress and Exposition, Vol. 85673, V011T11A041, 2021.

[14] Kurem E, Horuz I. A comparison between ammonia-water and water-lithium bromide solutions in absorption heat transformers. International Communications in Heat and Mass Transfer, 28(3), 427-438, 2001.

[15] Lin P, Wang RZ, Xia ZZ, Ma Q. Experimental investigation on heat transportation over long distance by ammonia–water absorption cycle. Energy Conversion and Management, 50(9), 2331-2339, 2009.

[16] Markmann B, Tokan T, Loth M, Stegmann J, Hartmann KH, Kruse H, Kabelac S. Experimental results of an absorption-compression heat pump using the working fluid ammonia/water for heat recovery in industrial processes. International Journal of Refrigeration, 99, 59-68, 2019.

[17] Mirl N, Schmid F, Bierling B, Spindler K. Design and analysis of an ammonia-water absorption heat pump. Applied Thermal Engineering, 165, 114531, 2020.

[18] Mumah SN, Adefila SS, Arinze EA. First law thermodynamic evaluation and simulation of ammonia-water absorption heat pump systems. Energy Conversion and Management, 35(8), 737-750, 1994.
[19] Villa G, Toppi T, Aprile M, Motta M. Performance improvement of gas-driven absorption heat pumps by controlling the flow rate in the solution branch. International Journal of Refrigeration, 145, 290-300, 2023.
[20] Wu T, Wu Y, Yu Z, Zhao H, Wu H. Experimental investigation on an ammonia–water–lithium bromide absorption refrigeration system without solution pump. Energy Conversion and Management, 52(5), 2314-2319, 2011.
[21] Younes MB, Altork Y, Shaban NA. Performance Evaluation of a Small Scale Ammonia-Water Absorption Cooling System for Off-Grid Rural Homes: A Numerical and Experimental Study. International Journal of Heat & Technology, 42(1), 2024.
[22] Zhou J, Li S. Simulation analysis of performance optimization of gas-driven ammonia-water absorption heat pump. Thermal Science, 24(6 Part B), 4253-4266, 2020.
[23] Zotter G, Rieberer R. Experimental analysis of a novel concept of a "thermally driven" solution pump operating a small-capacity ammonia/water absorption heat pumping system. International Journal of Refrigeration, 60, 190-205, 2015.
[24] Devlet Meteoroloji Genel Müdürlüğü. https://www.mgm.gov.tr/Veridegerlendirme/il-ve-ilceler-istatistik.aspx?m=ISPARTA (Erişim Tarihi: 2024).
[25] Klein SA. Engineering Equation Solver(EES), F-Chart Software, Version 10.835-3D. 2020

Uluslararası Teknolojik Bilimler Dergisi
International Journal of Technological Sciences
UTBD
IJTS

Araştırma Makalesi/Research Article

Termal enerji depolamalı parabolik güneş kolektörünün termodinamik incelenmesi

Pervin Alptekin[*1], **Reşat Selbaş**[2]

[1]Isparta Uygulamalı Bilimler Üniversitesi., Lisansüstü Eğitim Enstitisü, Enerji Sistemleri Müh. Anabilim Dalı, 32200, Türküye
[2]Isparta Uygulamalı Bilimler Üniversitesi, Teknoloji Fakültesi, Makine Mühendisliği Bölümü, 32200, Isparta

Anahtar Kelimeler
Güneş Enerjisi
Enerji Verimliliği
Ekserji verimliliği
Yenilenebilir Enerji Kaynağı
Termal Depolama

Makale geçmişi:
Geliş Tarihi: 03.07.2024
Kabul Tarihi: 25.12.2024

Öz: Günümüzde artan enerji ihtiyacını çevreye zarar vermesen karşılamak için yenilenebilir enerji kaynaklarına olan ilgi hızla artmaktadır. Bu çalışmada, Isparta ilinde kurulması planlanan bir parabolik güneş kolektörünün (PTC) enerji ve ekserji performansları incelenmiştir. Güneş enerjisinin kesintili yapısını dengelemek amacıyla sisteme bir termal enerji depolama (TES) birimi entegre edilmiştir. Matematiksel modelleme ve termodinamik analizler ile enerji ve ekserji verimlilikleri değerlendirilmiştir. Çalışmada, 2023 yılı Temmuz ayının 23. günü seçilmiş ve bu günde maksimum ışınım şiddeti 1050 W/m^2 olarak belirlenmiştir. Enerji verimliliği %47.1 ve ekserji verimliliği ise %16.68 olarak hesaplanmıştır. Tank hacminin de en iyi performansı 2 m^3 hacimde gösterdiği ve tank sıcaklığının 135.3 °C olduğu tespit edilmiştir. Işınım şiddetinin enerji verimliliği üzerindeki etkisi grafiklerle desteklenmiş ve önerilen sistemin Isparta ili için uygun bir çözüm sunduğu ortaya konulmuştur.

Atıf için/To Cite: Alptekin, P. Selbaş, R. Termal enerji depolamalı parabolik güneş kolektörünün termodinamik incelenmesi. Uluslararası Teknolojik Bilimler Dergisi, 16(2), 53-61, 2024.

Thermodynamic investigation of parabolic solar collector with thermal energy storage

Keywords
Solar Energy
Energy Efficiency
Exergy Efficiency
Renewable Energy Source
Thermal Storage

Article history:
Received: 03.07.2024
Accepted: 25.12.2024

Abstract: Nowadays, the interest in renewable energy sources is rapidly increasing in order to meet the increasing energy demand without harming the environment. In this study, the energy and exergy performances of a parabolic solar collector (PTC) planned to be installed in Isparta province are investigated. A thermal energy storage (TES) unit is integrated into the system to compensate for the intermittent nature of solar energy. Energy and exergy efficiencies are evaluated by mathematical modeling and thermodynamic analysis. In the study, the 23rd day of July, 2023 was selected and the maximum irradiance on this day was determined as 1050 W/m^2. Energy efficiency was calculated as 47.1% and exergy efficiency as 16.68%. It was also found that the tank volume showed the best performance at a volume of 2 m^3 and the tank temperature was 135.3 °C. The effect of radiation intensity on energy efficiency is supported with graphs and it is shown that the proposed system offers a suitable solution for Isparta province.

1. Giriş

Ülkelerin gelişmesiyle birlikte insanların enerjiye olan ihtiyacı sürekli olarak artmaktadır. Özellikle gelişmekte olan ülkelerde bu ihtiyaç daha fazladır. Öte yandan, bu ihtiyacı karşılamak için fosil yakıtların kullanılması zorlukları da beraberinde getirmektedir [1]. Fosil yakıt rezervleri sınırlıdır ve bu kaynakların yakılması küresel ısınma gibi çeşitli çevresel sorunlara yol açmaktadır [2].

Enerjinin ekonomik büyüme, kamu politikası, ulusal güvenlik ve devlet gelirleri gibi çeşitli hususlar

* İlgili yazar/Corresponding author: prvnalptekin@gmail.com

üzerindeki tartışmasız etkisi iyi bilinmektedir [3]. Günümüzde, Dünyadaki enerji üretiminin önemli bir kısmı fosil yakıtlardan kaynaklanmaktadır ve bu en ideal senaryo değildir. Bu durum, küresel ısınmayı sanayi öncesi döneme kıyasla 2 °C 'nin altında bir seviyede sınırlama hedefini öngören Paris İklim Anlaşması ile birlikte sıcaklık artışını aynı ölçütün üzerinde 1.5 °C ile daha da sınırlamaya odaklanır [4]. Fosil kaynaklar tükenmekte ve tüketimden kaynaklanan karbon emisyonları da eş zamanlı olarak artmaktadır. Bu nedenle, birçok ülke sürdürülebilir bir alternatif olarak yenilenebilir enerjiyi giderek daha fazla ilgi göstermektedir. En umut verici temiz enerji kaynaklarından biri, emisyonu olmayan sınırsız bir kaynak olan güneş enerjisidir [4]. Yenilenebilir enerji kaynaklarının birçok çeşidi vardır. Ancak güneş enerjisi en çok kullanılandır çünkü bulunması kolaydır ve çevre üzerinde en az etkiye sahiptir [5].

Güneş enerjisi, güneş PV ve güneş termal olmak üzere iki teknolojiye ayrılmaktadır. Birincisi önemli ölçüde ilgi çekmesine rağmen ikincisinin yaygınlaşmasında kayda değer bir artış olmuştur [4]. Yenilenebilir enerji kaynağı olarak güneş enerjisi, kullanım ömrü boyunca enerji sağlama potansiyeline sahiptir. Güneş enerjisi teknolojisinden bir olan parabolik güneş kolektörleri, yüksek sıcaklıklara ulaşarak sıcak su ve elektrik üretebilir. Parabolik oluklu güneş kolektörlerini kullanmanın potansiyel avantajı, evde ve işyerinde kullanılabilmelerinin yanı sıra bunlardan büyük çapta elektrik üretilebilmesidir [5].

Güneş kolektörleri, soğutma, damıtma, ısıtma ve endüstriyel proseslerde enerji giderlerini azaltmak için kullanılmakta ve yüksek sıcaklık uygulamalarında geniş kullanım alanı bulunmaktadır [5]. Parabolik oluklu yoğunlaştırılmış güneş enerjileri (CSP) gelişmiş teknolojilerdir ve Güney Kaliforniya'nın Mojave Çölü'nde dokuz Güneş Enerjisi Elektrik Üretim Sisteminin (SEGS) inşa edildiği 1980'lerden beri kullanılmaktadır. Bu SEGS tesisleri toplam 354 MW kurulu güç kapasitesine sahiptir ve %10'luk bir verimlilik elde etmiştir. Bu nedenle parabolik oluk CSP sistemleri, diğer tüm CSP tesis türleriyle karşılaştırıldığında en gelişmiş ve ticari olarak kanıtlanmış teknoloji olarak kabul edilmektedir [6]. PTC sistemi, yoğunlaştırılmış güneş ışınımı ile alıcı tüpteki ısı emici akışkanı ısıtır. Elde edilen termal enerji daha sonra genellikle bir ısı transfer akışkanı (HTF) kullanılarak bir termal enerji depolama (TES) tankına aktarılır daha sonra kullanılmak üzere enerjinin depolanması sağlanır. Güneş enerjisinin yoğunlaştırılması ve TES'in birleşimi, güneş ışınlarının yoğun olmadığında bile sürekli enerji üretimine olanak sağlar ve önerilen sistemin genel verimliliğini ve güvenirliliğini artırır [7],[8]. TES'in nasıl çalıştığına dair şu örnek verilebilir, güneş enerjisi gün boyunca akşam saatlerinde ısıtma için depolanabilirken, yaz aylarında serin hava sağlamak için kış aylarında soğuk hava depolanabilir [9].

Enerji depolama teknikleri kimyasal (örneğin; hidrojen depolama, amonyak depolama ve sentetik doğal gaz), elektriksel (örneğin; süper kapasitörler), mekanik (örneğin; volan ve sıkıştırılmış hava) ve termal (örneğin; termo-kimyasal, hissedilebilir ısı, gizli ısı) olmak üzere çeşitli yöntemlerden oluşmaktadır [10]. Bir enerji depolama seçeneği olarak, soğuk ve ısı depolamayı içeren termal enerji depolama, iklimlendirme, soğutma ve sıcak su gibi çok çeşitli uygulamalar için giderek daha popüler hale gelmektedir [11].

Önerilen bu sistemin amacı, Isparta ili için kesintisiz yenilenebilir enerji sağlamak üzere termal depolama teknolojisi kullanarak sürdürülebilir bir sistem modellemektir. Bu modelleme, meteorolojik verilere dayalı saatlik dinamik analizler ve termodinamik değerlendirmeler ile sistemin performansı üzerinde etkili olan önemli ana parametrelerin etkilerini ortaya koymaktadır.

2. Sistem Tanımı

Yapılan bu çalışmada ele alınan sistem, temiz enerji üretimi için güneş enerjisi teknolojilerinden biri olan parabolik oluk kolektörü, depolama tankı ve pompadan oluşan bir sistem modellenmiştir. Sistemin modellemesi ve performans analizleri Engineering Equation Solver programı yardımıyla yapılacaktır. Şekil 2.1'de görüldüğü gibi sistemin şematik gösterimi verilmiştir.

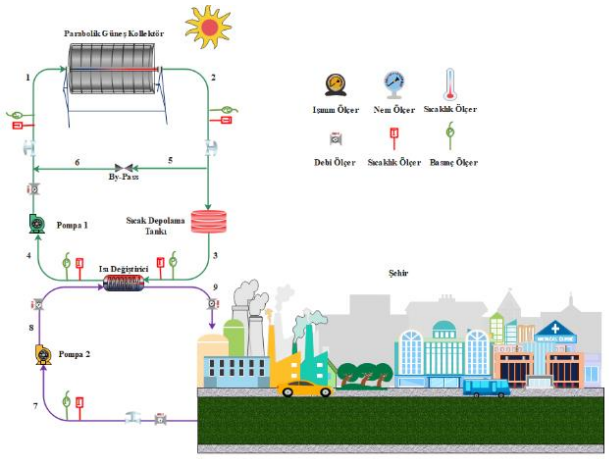

Şekil 2.1. Tasarlanan sistemin şematik gösterimi.

Güneş enerjisinden elde edilen ısıl enerji, ısıl depolama tankı içerisinde akışkan ile karışmadan bir ısı değiştirici vasıtasıyla transfer edilmektedir. Depolama tankından çıkan akışkan doğal sirkülasyon ile ısı değiştiriciye yönlendirilerek enerji aktarımı gerçekleştirilmektedir. Parabolik kolektörde çalışma akışkanı olarak Slytherm 800 tercih edilmiştir. Slyherm 800, -40 °C ile 400 °C arasındaki sıcaklık aralığında sıvı fazda çalışabilme özelliğine sahiptir [13]. Isı değiştiricisinden aktarılan enerji, sıcak akışkanın şehirde kullanılmasını sağlamaktadır. Enerjisini aktaran akışkan, pompa yardımıyla tekrar sisteme geri döndürülerek çevrim tamamlanmaktadır.

Sistemin enerji ve ekserji analizini gerçekleştirilmesi için bazı verilerin kabul edilmesi gerekmektedir. Çalışmada kullanılan parametreler Çizelge 2.1'de sunulmuş olup, mühendislik hesaplaması için EES programı kullanılmıştır.

Termodinamik enerji ve ekserji analizlerinin yapılırken aşağıdaki kabuller esas alınmıştır.

- Isı değiştiriciler ve pompalar adyabatik kabul edilmiştir.
- Ekserji hesabı yapılırken kinetik, potansiyel ve kimyasal enerjileri ve ekserjileri ihmal edilmiştir.
- Tüm sistem sürekli akışlı açık olarak tasarlanmıştır.
- Referans koşullarında sıcaklık değeri 25 °C ve basınç değeri 101.325 kPa olarak kabul edilmiştir.
- Her bir kompenentin basınç düşümü ihmal edilmiştir.
- Türbin ve pompalar izentropik kabul edilmiştir.

Tablo 2.1'de parabolik kolektörünün tasarım parametreleri verilmiştir.

Tablo 2.1. Parabolik kolektör tasarım parametreleri [12].

Parametre	Değer
Genişlik (m)	1.788
Uzunluk (m)	6
Odak uzunluğu (m)	0.3276
Açıklık alanı (m^2)	10.73
Alıcı iç boru çapı (m)	0.034
Alıcı dış boru çapı(m)	0.038
Cam dış çapı (m)	0.01
Cam iç çapı (m)	0.016
Cam ışınım yayma oranı	0.86
Cam ışınım geçirme oranı	0.935
Absorber ışınım yutma oranı	0.96
Açıklık alan yansıtma oranı	0.826
Absorber ışınım yayma katsayısı	0.097
Maksimum optik verim	0.75

3. Matematiksel Modelleme

Bu bölümde, Isparta koşullarında Meteonorm [18] veri tabanından elde edilen verileri kullanarak parabolik oluk kolektörünün dinamik modellenmesi gerçekleştirilecek ve tasarlanan çevrimin termodinamiğin birinci ve ikinci yasalarına dayalı enerji ve ekserji analizi gerçekleştirilecektir. Modellemede kullanılan diferansiyel denklemler, ısıl verimlilik gibi önemli parametreler ise detaylı bir şekilde sunulacaktır.

Yatay düzleme gelen toplam güneş radyasyonu, yalnızca direkt güneş radyasyonunun parabolik oluk kolektörünün alıcı yüzeyine düşen bileşenidir. Bundan dolayı yoğunlaştırıcı üzerine gelen güneş radyasyonu miktarı (W/m^2) Denklem (1) ile hesaplanmaktadır [12].

$$Q_s = A_a . G_b \quad (1)$$

Burada, G_b (W/m^2) olarak gelen eğik yüzeye gelen direkt güneş radyasyon değeridir. A_a (m^2) parabolik açıklık alanıdır. Güneş radyasyonu miktarı ile güneş enerjisi faydalı ısı miktarı oranı ile ısıl verim aşağıdaki denklem (2) ile hesaplanmaktadır [12].

$$\eta_{th} = \frac{Q_u}{Q_s} \quad (2)$$

Isıl verim hesaplanması için gerekli deneysel verilerden elde edilen parametreler kullanılarak hesaplamalar yapılmaktadır. Denklem (3) ile termal verimlilik (ısıl verim) hesaplanmaktadır.

$$\eta_{th} = 0.7408 . K(\theta) - 0.0432 . \left(\frac{T_g - T_{ort}}{G_b}\right) \quad (3)$$

Burada, K(θ) direk ışınım geliş açısına bağlı olarak kaynaklanan hataları içeren geliş açısı düzeltme ile bağlantılı denklem (4) ile hesaplanır [12].

$$K(\theta) = \cos(\theta) - 5.25097.10^{-4}.\theta - 2.859621.10^{-5}.\theta^2 \quad (4)$$

Geliş açısı hesaplanması denklem (5) ile bulunmaktadır [12].

$$\cos(\theta) = \sqrt{cos^2(\theta_z) + cos^2(\delta).sin^2(\omega)} \quad (5)$$

Geliş açısı hesaplanması için denklikasyon açısı hesaplanması gereken parametrelerden biridir. Denklem (6) ile bulunmaktadır. DD yıl içindeki numarasıdır. Örneğin DD=1 Ocak şeklindedir [12].

$$\delta = 23.45.sin(2\pi \frac{284+DD}{365}) \quad (6)$$

Geliş açısı hesaplanmasında bir diğer parametre güneş zenit açısıdır. Denklem (7) ile hesaplanabilmektedir [12].

$$cos(\theta_z) = sin(\varphi).sin(\delta) + cos(\varphi).cos(\delta).cos(\omega) \quad (7)$$

Güneş açısı, saat cinsinden güneş zamanı (t_h) kullanılarak aşağıdaki denklem (8) ile belirlenmektedir [12].

$$\omega = 15.(t_h - 12) \quad (8)$$

Faydalı ısı miktarını bulmak için iki yol kullanılmaktadır. Bunlardan birincisi enerji dengesi denklem (9) ile hesaplanır [13].

$$Q_u = \dot{m}.c_p.(T_ç - T_g) \quad (9)$$

Burada, $T_ç$ve T_g akışkanın giriş ve çıkış sıcaklığını ifade etmektedir. Bir diğer yol ise absorber boru ile akışkan arasındaki ısı transfer kullanılarak denklem (10) ile hesaplanmaktadır [13].

$$Q_u = A_{ro}.h.(T_r - T_{fm}) \quad (10)$$

Burada, A_{ro} (m^2) borunun kesit alanı, T_r (°C) absorber yüzey sıcaklığı, T_{fm} (°C) ortalama akışkan sıcaklığıdır. Isı transfer katsayısı nusselt sayısı kullanılarak denklem (11) ile bulunmaktadır [13].

$$h = \frac{Nu.k}{D_{ri}} \quad (11)$$

k ısı iletim katsayısı (W/m^2) dır. Nusselt sayısı için Reynolds sayısı (Re) belirlenir. Denklem (12) ve denklem (13) ile hesaplanır [14].

$$Re>2300 \qquad N_u = 0.023Re^{0.8}Pr^{0.4} \quad (12)$$

$$Re<2300 \qquad N_u = 4.364 \quad (13)$$

Reynolds sayısı (Re) denklem (14) ile hesaplanmaktadır [15].

$$Re = \frac{4\,m}{\pi.D_{ri}\,\mu} \quad (14)$$

Burada, μ dinamik vizkozite (Pa s) dir. Ortalama akışkan sıcaklığı denklem (15) ile bulunmaktadır [13].

$$T_{fm} = \frac{T_g + T_ç}{2} \quad (15)$$

Kararlı durum koşullarında, emicinin cama olan termal kayıpları, camın ortama olan termal kayıplarına eşittir. Denklem (16) ile hesaplanır [13].

$$Q_{kay} = A_{co}.\sigma.\varepsilon_c.(T_c^4 - T_{çev}^4) + A_{co}\,.\,h_{dış}.(T_c^4 - T_{gök}^4) \quad (16)$$

Burada, σ (W/m^2K^4) Stefan-Boltzmann katsayısıdır ve değeri $5{,}67.10^{-8}$ dir. T_c cam yüzeyin sıcaklığı ve $h_{dış}$ (W/m^2K) cam dış yüzeyindeki ısı taşınım katsayısıdır. $T_{gök}$ ortam sıcaklığına bağlı olarak hesaplanan gökyüzü sıcaklığıdır. Denklem (17) ile hesaplanır [13].

$$T_{gök} = 0.0552.T_{çev}^{1.5} \quad (17)$$

Cam ve ortam arasındaki ısı taşınım katsayısı rüzgâr hızına bağlı olarak denklem (18) ile hesaplanır [13].

$$h_{dış} = 4.V^{0.58}.D_{co}^{-0.42} \quad (18)$$

Absorber üzerindeki enerji dengesi denklem faydalı güneş enerjisi ve termal kayıpların toplamına eşittir. Denklem (19) ile bulunmaktadır [13].

$$Q_{abs} = Q_u + Q_{kay} \quad (19)$$

Ekserji verimi denklem (20) ile hesaplanmaktadır. Yararlı ekserji üretiminin (E_u), güneş ışınımının ekserji akışına (E_s) oranı ile belirlenir [13].

$$\eta_{ex} = \frac{E_u}{E_s} \quad (21)$$

Yararlı ekserji üretiminin (E_u) denklem (22) ile hesaplanır. Sıcaklıklar denklemde Kelvin cinsinden yazılır [13].

$$E_u = Q_u - m.cp.T_o\,.\,ln[\frac{T_ç}{T_g}] - \frac{m.T.\Delta P}{\rho.T_{fm}} \quad (22)$$

Güneş ışınımının ekserji akışına (E_s) denklem (23) ile hesaplanır. Sıcaklıklar denklem de Kelvin cinsinden yazılır [13].

$$E_s = Q_s.[1 - \frac{4}{3}.\frac{To}{T_{güneş}} + \frac{1}{3}\,.\,(\frac{T_o}{T_{güneş}})^4] \quad (23)$$

Referans sıcaklık (T_o) 298.15 K ve güneş dış yüzey sıcaklığı ($T_{güneş}$) 5770 K olarak seçilmiştir. Enerji verimliliği denklem (24) ile hesaplanır [13].

$$\eta_{enerji} = \frac{Q_u - \frac{W_p}{\eta_{el}}}{Q_s} \quad (24)$$

Termal enerji depolama tankından bulunan bir ısı değiştirici ile tank içerisindeki akışkanın karışmadan enerjisini aktardığı kabul edilmiştir. Termal kayıp katsayısı (U_T), yalıtım depolama tankları için tipik bir değer olan 0.5 W/m^{2}K'ne eşit alınmıştır. Denklem (25) ile hesaplanır [12].

$$\frac{\rho.V}{n}.c_p.\frac{dT_s}{dt} = m.c_p.(T_ç - T_s) - U_T.A_T.(T_s - T_{ort}) \quad (25)$$

Kararlı durum tankta depolanan enerji ($\dot{Q}_{depolanan}$) sıfıra eşit olur. Tanktan dış ortama olan ısı kaybı denklem (26) ile hesaplanmaktadır [12].

$$\dot{Q}_{kay,tank} = U_T.A_T.(T_s - T_{ort}) \quad (26)$$

Tankın yüzey alan hesabı denklem (27) ile hesaplanır [12].

$$A_T = \frac{\pi.D_T^2}{4} + \pi.D_T.L_T \quad (27)$$

Burada, D_T tank çapı, L_T tank uzunluğunu ifade etmektedir. Depolama tankı hacmi boyutları ile ilişkilendiren denklem (28) ile bulunmaktadır [12].

$$V = \frac{\pi.D_T^2}{4}.L_T \quad (28)$$

Sıcak akışkan ısı miktarı denklem (29) ile hesaplanır. Soğuk akışkan ısı miktarı denklem (30) ile hesaplanır. Ortalama ısı miktarı denklem (31) ile hesaplanmaktadır [16].

$$\dot{Q}_h = \dot{m}_h.c_{ph}.(T_{h,g} - T_{hç}) \quad (29)$$

$$\dot{Q}_c = \dot{m}_c.c_{pc}.(T_{c,ç} - T_{c,g}) \quad (30)$$

$$\dot{Q}_{ort} = (\dot{Q}_h + \dot{Q}_c)/2 \quad (31)$$

Burada,$T_{h,g}$ ve $T_{h,ç}$ sıcaklıkları, sırasıyla sıcak akışkanın ısı transferi gerçekleştiren sistemdeki giriş ve çıkış sıcaklıklarını temsil etmektedir. $T_{c,g}$ ve $T_{c,ç}$ soğuk akışkanın giriş ve çıkış sıcaklıklarını, $\dot{Q}_h$ sıcak akışkan tarafından taşınan ısı miktarını, $\dot{Q}_c$ soğuk akışkan tarafından alınan ısı miktarını ifade etmektedir. Ayrıca $\dot{Q}_{ort}$ ortalama ısı miktarını ve $\dot{Q}_{\text{maks}}$ ise üretilebilecek maksimum ısı miktarını ifade etmektedir. Denklem (32) ile belirlenmektedir [17].

$$\dot{Q}_{maks} = c_{min}.(T_{h,g} - T_{c,g}) \quad (32)$$

Burada, ısıl kapasitelerin hangisi küçük ise onun kullanılması ile $\dot{Q}_{maks}$ bulunur. Isıl kapasitelerin hesabı aşağıdaki denklem (33) ve denklem (34) ile bulunur [17].

$$C_{ph} = \dot{m}_h.c_{ph} \quad (33)$$

$$C_{pc} = \dot{m}_c.c_{pc} \quad (34)$$

Toplam ısı transfer miktarı (U) aşağıdaki denklem (35) ile hesaplanır [16].

$$U = \frac{\dot{Q}_{ort}}{A.LMTD} \quad (35)$$

Burada, LMTD logaritmik ortalama sıcaklık farkını temsil eder. Bu çalışmada ters akışlı plakalı ısı değiştiricinin ortalama logaritmik sıcaklık değeri (ΔT_m) denklem (36) ile hesaplanır [16].

$$LMTD = \frac{\Delta T_{maks} - \Delta T_{min}}{ln\frac{\Delta T_{maks}}{\Delta T_{min}}} \quad (36)$$

$$LMTD = \frac{(T_{h,ç} - T_{c,g}) - (T_{h,g} - T_{c,ç})}{\ln\frac{(T_{h,ç} - T_{c,g})}{(T_{h,g} - T_{c,ç})}} \quad (37)$$

Isı değiştiricinin etkenliği, ortalama ısı miktarı ile maksimumum ısı miktarı oranı şeklinde denklem (38) ile hesaplanır [17].

$$\varepsilon = \frac{\dot{Q}_{ort}}{\dot{Q}_{maks}} \quad (38)$$

4. Araştırma Bulguları

Isparta ili koşullarında enerji talebini karşılamak amacıyla tasarlanan güneş enerjisi destekli termal enerji depolama sisteminin matematiksel modellemesi yapılmış ve sistem termodinamik performans açıdan detaylı incelenmiştir. Parabolik güneş kolektöründen elde edilen enerji, üretildikten sonra şehirdeki enerji ihtiyacını karşılamak için kullanılabilmektedir.

Tasarlanan sistemin temel çalışma parametreleri belirlenirken 2023 yılına ait Temmuz 23 günü seçilmiştir. 23 Temmuz'un seçilme nedeni, güneş ışınımının en yüksek seviyelere ulaştığı ve yazın en sıcak, güneş ışınımın en yoğun olduğu dönemi temsil etmektedir. Temmuz 23 gününe ait güneş ışınım şiddeti, güneşlenme süresi, çevre sıcaklığı ve rüzgâr hızı verileri faydalanılmıştır. Isparta ilinin 2023 yılına ait aylık ortalama güneş ışınım şiddeti değişimi şekil 4.1'de sunulmuştur [18].

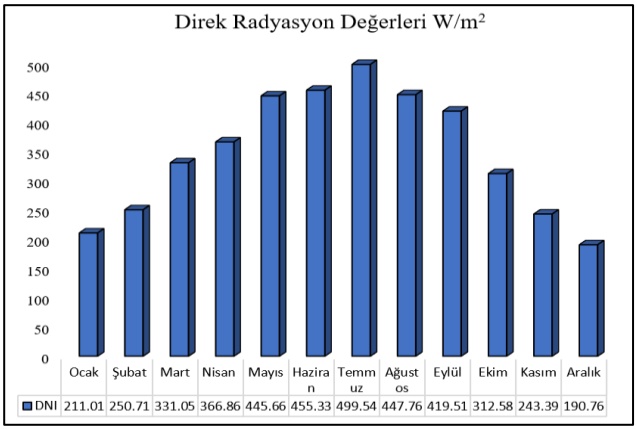

Şekil 4.1. 2023 yılı Isparta koşullarında aylık ortalama güneş ışınım şiddeti değişimi [18].

Şekil 4.2'de Isparta iline ait 2023 yılı Temmuz ayına ilişkin ortalama güneş ışınımındaki dağılımı gösterilmektedir.

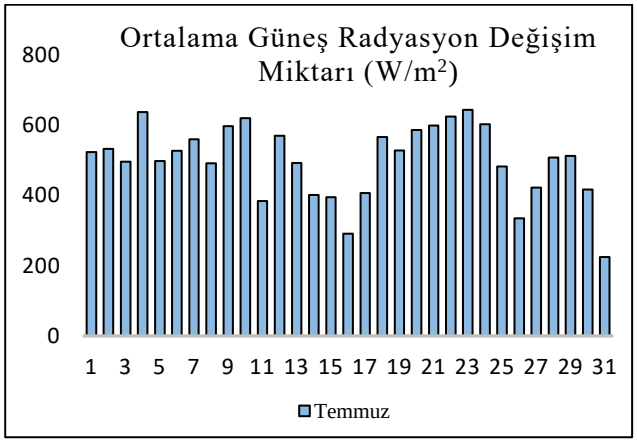

Şekil 4.2. 2023 yılı Temmuz ayının ortalama güneş ışınımı dağılımı [18].

Şekil 4.3. Çeşitli geliş açıları için kolektörün giriş açısındaki değişimi gösterilmiştir. Grafik incelendiğinde, 40°'den sonra geliş açısının parabolik bir şekilde azaldığı görülmektedir. 90°'de ise *K(θ)* sıfır değerine ulaşmıştır. Geliş açısındaki değerlerin kademeli olarak düşmesi, düşük termal ve ekserjetik verimliliklere yol açtığı gözlemlenmiştir.

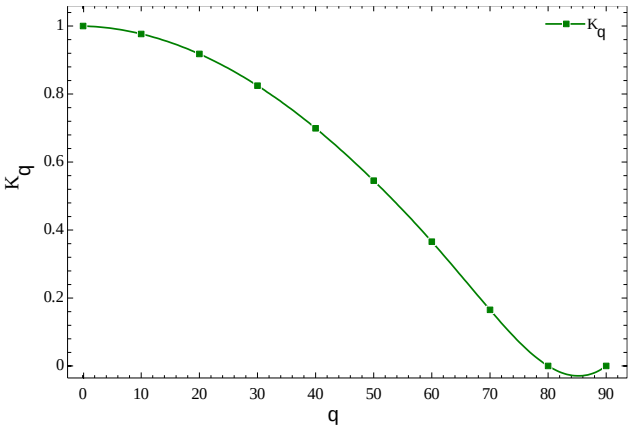

Şekil 4.3. Çeşitli geliş açıları için kolektörün giriş açısındaki değişim.

Şekil 4.4'de Tank hacminin değişimine bağlı olarak tank sıcaklığında meydana gelen değişim sunulmuştur. Daha küçük depolama tankı hacimlerinde, daha yüksek tank sıcaklıklarının elde edildiği tespit edilmiştir. 2 ile 12 m^3 tank hacimleri aralığında en yüksek tank sıcaklığı 2 m^3 de olduğu grafik göstermektedir. 2 m^3 de tank sıcaklığı 135.3 °C iken 12 m^3 de 131.6 °C sıcaklıklar elde edilmiştir.

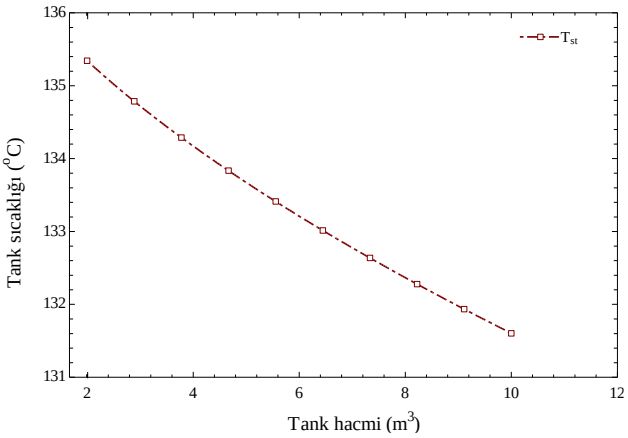

Şekil 4.4. Tank hacminin değişimine bağlı olarak tank sıcaklığının değişimi.

Rüzgâr hızının değişimine göre sistemin enerji ve ekserji verimliliği üzerindeki etkisi şekil 4.5'de gösterilmektedir. Grafikten elde edilen sonuca göre rüzgâr hızının artması, sistemin enerji ve ekserji verimliliği üzerinde olumlu etkisi olduğunu göstermektedir. Bunun sebebi, yazın sıcak havalar da rüzgârın hava akışını sağlayarak ortam sıcaklığında meydana gelen azalmadan dolayı güneş kolektörünün ısınmasını engellemesinden kaynaklanmaktadır.

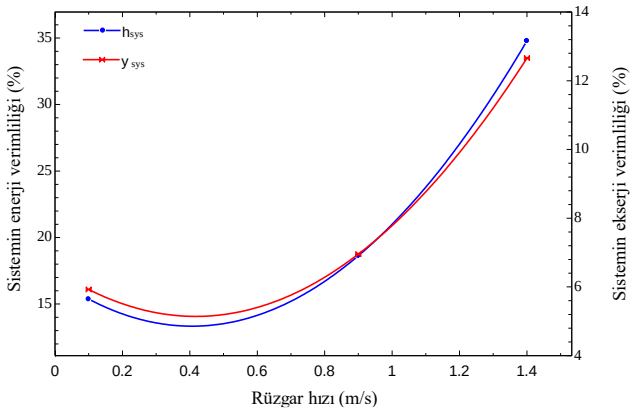

Şekil 4.5. Rüzgâr hızının değişimine göre sistemin enerji ve ekserji verimliliği üzerindeki etkisi.

Şekil 4.6'da 2023 yılının Temmuz 23 gününde saatlik olarak güneş ışınım şiddetinin değişim miktarı verilmiştir. En düşük ışınım şiddeti 06:00'da 80 W/m², en yüksek ışınım şiddeti 13:00'de 1050 W/m² olarak belirlenmiştir.

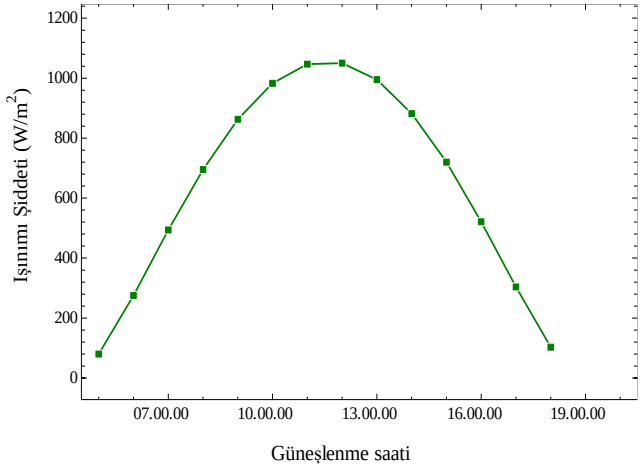

Şekil 4.6. Güneşlenme saatine bağlı olarak güneş radyasyon miktarının değişimi.

Şekil 4.7'de görüldüğü gibi ışınım şiddetinin değişimi ile sistemin enerji ve ekserji verimliliklerin değişimi verilmiştir. Işınım şiddeti arttıkça doğru orantılı olarak enerji ve ekserji verimliliği de artmıştır. Güneş ışınım şiddetinin artması ile enerji verimliliği %18.63'ten %47.1' e artış gösterdiği tespit edilmiştir. Ekserji verimliliği %6.95'den %16.68'e çıkmıştır.

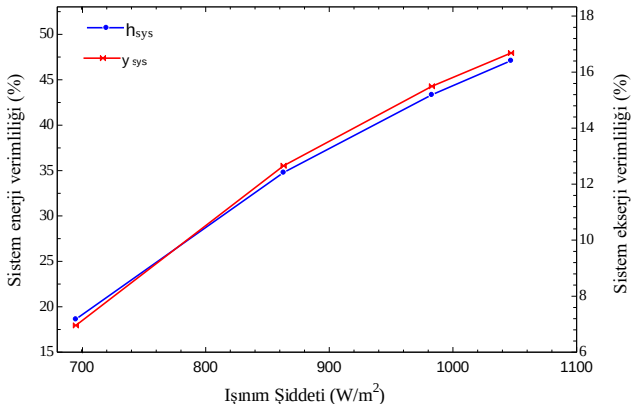

Şekil 4.7. Işınım şiddetinin değişimine göre sistemin enerji ve ekserji verimliliği üzerindeki etkisi.

Farklı ışınım şiddetine göre sistemin elemanlarının kapasitelerindeki değişimi şekil 4.8'de gösterilmiştir. Güneş radyasyon miktarı arttıkça sistem kapasitelerin üzerinde olumlu etkisi olmuştur ve güneş radyasyon miktarı arttıkça elemanların kapasitelerinin arttığı görülmüştür. Güneş radyasyonu artması ile faydalı enerji miktarı 4203 W'dan 6375 W' a bir artış göstermiştir. Isı değiştirici miktarı 783.1 W'dan 3003 W'lık bir artış meydana geldiği belirlenmiştir.

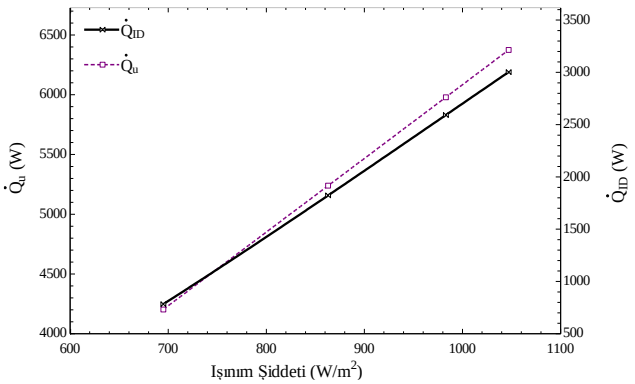

Şekil 4.8. Işınım şiddetinin değişiminin yararlı enerji ve ısı değiştirici üzerindeki etkisi.

Şekil 4.9'de parabolik güneş kolektörünün enerji ve ekserji verimliliğinin ışınım şiddetine göre değişimi verilmiştir. Işınım şiddeti arttıkça parabolik güneş kolektörün enerji ve ekserji verimliliği lineer olarak artış göstermiştir. Işınım şiddetinin değişimi ile enerji verimliliği ve ekserji verimliliği sırasıyla %56.75, %14.53 olarak tespit edilmiştir.

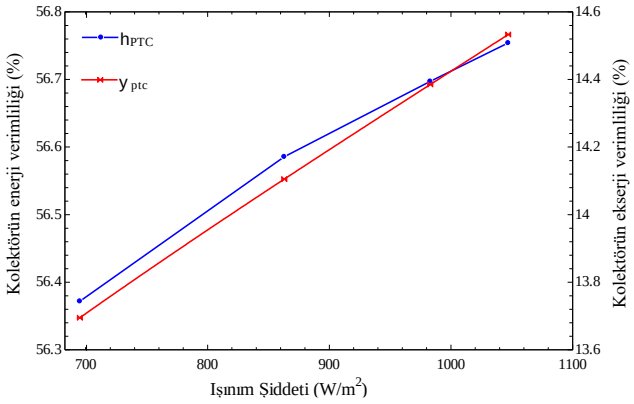

Şekil 4.9. Kolektörün enerji ve ekserji verimliliğinin ışınım şiddetine göre değişimi.

5. Sonuçlar

Bu çalışmada güneş enerjisi kaynaklı PTC sisteminin modellemesi ile sistemin enerji ve ekserji analizi incelenmiştir. Meteonorm'dan alınan verileri göre, saat 13:00'da 1050 W/m^2 ile en yüksek ışınım şiddetinin elde edildiği gözlemlenmiştir. Meteorolojik verileri kullanılarak, ışınım şiddeti, ortam sıcaklığı, rüzgar hızı gibi faktörler ile analizler yapılmıştır. PTC sistemin enerji ve ekserji verimliliği sırasıyla %56.75 ve %14.53 olarak belirlenmiştir. Yararlı enerji miktarı 6375 W, ısı değiştiricinin ürettiği ısı miktarı 3003 W olarak hesaplanırken, genel enerji verimliliği %47.1, ekserji verimliliği %16.68 olarak tespit edilmiştir. Tank haminin 4 m^3 olduğu ve tank sıcaklığının 134.2 °C olarak belirlendiği gözlemlenmiştir.

Çalışmada, PTC destekli bir sistemin Isparta ilinde kurulabilirliği ve uygulanabilirliğine yer verilmiştir. Kesintili güneş enerjisinin fazla enerji üretildiği zamanlarda, termal depolama ünitesi ile uzun süreli kullanım sağlanmaması hedeflenmiştir. Yapılan analizlerde, Isparta ilinin saatlik ışınım verileri incelenmiş ve bölgenin yüksek ışınım şiddeti potansiyeline sahip olduğu tespit edilmiştir. Parametrik çalışmalar yapılarak sistem üzerindeki etkiler detaylı bir şekilde analiz edilmiştir. Yenilenebilir enerji kaynaklarının kullanımı ile sera gazı salınımının büyük oranda azaltılması, sistem verimliliğinin artırılması hedeflenmiştir. Yenilenebilir enerji teknolojilerinin gelişimiyle birlikte sistemin gelecekteki potansiyelini artırabileceğini vurgulanmıştır. Modellin geliştirilmesi durumunda, sisteme Organik rankine çevrimi (ORC) entegre edilerek elektrik üretimi yapılabilmesi mümkün olabileceği düşünülmektedir.

Teşekkür: 2022-YL1-0183 numaralı 'Termal enerji depolamalı parabolik güneş kolektörünün termodinamik incelenmesi' adlı proje ile makalemin maddi olarak destekleyen Isparta Uygulamalı Bilimler Üniversitesi Bilimsel Araştırma Projeleri (BAP) Yönetim Birimi Başkanlığı'na teşekkür ederim.

Kaynaklar

[1] Mohseni M, Hajinezhad A, Moosavian SF. Thermodynamic analysis and multi-objective optimization of an ORC-based solar-natural gas driven trigeneration system for a residential area. Case Studies in Thermal Engineering. 59(104513), 2024.

[2] Murugan S, Horák B. Tri and polygeneration systems-A review. Renewable and Sustainable Energy Reviews, 60, 1032-1051, 2016.

[3] Heidari A, Aslani A, Hajinezhad A, Tayyar SH. Strategic analysis of Iran's energy system. Strategic Planning for Energy and the Environment, 37(1), 56-79, 2017.

[4] Zaharil HA, Yang H. Thermodynamic analysis of a parabolic trough power plant integrating supercritical carbon dioxide Brayton cycle and direct contact membrane distillation. Applied Thermal Engineering, 123637, 2024.

[5] Cetiner C. Thermal analysis of operating a solar-powered diffusion absorption refrigerator with a parabolic collector. Case Studies in Thermal Engineering, 53(103893), 2024.

[6] AlZahrani AA, Dincer I. Energy and exergy analyses of a parabolic trough solar power plant using carbon dioxide power cycle. Energy conversion and management, 158, 476-488, 2018.

[7] Achkari O, El Fadar A. Latest developments on TES and CSP technologies – energy and environmental issues, applications and research trends, Applied Thermal Engineering, 167 (114806), 1-31, 2020. https://doi.org/10.1016/j.applthermaleng.2019.114806

[8] Shabgard H, Rahimi H, Naghashnejad M, Acosta PM, Sharifi N, Mahdavi M, Faghri A. Thermal energy storage in desalination systems: state of the art, challenges and opportunities. J. Energy Storage 52 (104799), 1-30, 2022. https://doi.org/10.1016/j.est.2022.104799.

[9] Batgi SU, Dincer I. Design of a two-renewable energy source-based system with thermal energy storage and hydrogen storage for sustainable development. Journal of Energy Storage, 89(111742), 2024.

[10] Erdemir D, Dincer I. A new solar energy-based system integrated with hydrogen storage and heat recovery for sustainable community. Sustainable Energy Technologies and Assessments, 52(102355), 2022. https://doi.org/10.1016/j.seta.2022.102355.

[11] Powell KM, Edgar TF. Modeling and control of a solar thermal power plant with thermal energy

storage. Chem. Eng. Sci. 71 138–145, 2012. https://doi.org/ 10.1016/j.ces.2011.12.009.
[12] Bellos E. Tzivanidis C. Belessiotis V. Daily performance of parabolic trough solar collectors. Solar Energy, 158, 663-678, 2017.
[13] Bellos, E, Tzivanidis C. Enhancing the performance of evacuated and non-evacuated parabolic trough collectors using twisted tape inserts, perforated plate inserts and internally finned absorber. Energies, 11(5), 1-28, 2018.
[14] Kizilkan O, Khanmohammadi S, Saadat-Targhi M. Solar based CO2 power cycle employing thermoelectric generator and absorption refrigeration: Thermodynamic assessment and multi-objective optimization. Energy conversion and management, 200(112072), 2019.
[15] Bellos E, Tzivanidis C. Parametric analysis and optimization of an Organic Rankine Cycle with nanofluid based solar parabolic trough collectors. Renewable Energy, 114, 1376-1393, 2017.
[16] Zheng D, Wang J, Chen Z, Baleta J, Sundén B. Performance analysis of a plate heat exchanger using various nanofluids. International Journal of Heat and Mass Transfer, 158(119993), 2020.
[17] Islam MS, Xu F, Saha SC. Thermal performance investigation in a novel corrugated plate heat exchanger. International journal of heat and mass transfer, 148(119095), 2020.
[18] Meteonorm. https://meteonorm.com, (Erişim Tarihi: 31.12.2023).